Chapter 7

THE ACCELERATION SYSTEMS

Contents

7.1   Introduction

In this chapter we discuss the systems for acceleration of muons from the low-energy output of the cooling system ($\approx 0.1\,\text{GeV}$) to full energy at $2\,\text{TeV}$, where the muons are transferred to storage in the collider ring. We first describe the requirements of the acceleration system. The most critical of these is that the muons must be accelerated before they decay, which sets limitations on the acceleration rate, and constrains the potential form of acceleration systems, although the lifetime is sufficiently long to enable multipass systems. Other requirements include phase-space matching from the output of the cooling system to the collider, and beam acceptances. We then describe potential acceleration systems, which include full-energy linac, rapid-cycling synchrotron and recirculating-linac options. Because it appears most readily obtainable within existing technology, our current baseline acceleration choice is a sequence or cascade of recirculating linacs, each of which increases beam energy by about an order of magnitude and accommodates bunch length reductions by almost as much. We present a candidate scenario. Results of particle tracking in this candidate choice provide a *proof of principle* of the general approach. We then describe in some detail the required rf systems and beam transports. Optimization considerations and possible variations are discussed. Difficulties associated with injection from the cooling system are also discussed; a single-pass $\approx 1\,\text{GeV}$ linac tailored for matching from cooling into the first recirculating linac will be required. Other acceleration scenarios, which include rapid-cycling magnetic fields, are also described and their potential advantages are discussed, as well as the technology developments needed for their implementation. It is probable that an optimal system will incorporate rapid-cycling in some portion of its acceleration system.

7.2   Constraints and Requirements

The central difficulty in a $\mu^+\mu^-$ collider is that muons decay, and the muons must be collected, cooled, accelerated, and collided within their limited lifetimes. The lifetime is sufficient to permit multipass acceleration and collisions, but that lifetime must be carefully budgeted to avoid excessive decay. An accompanying problem is that muons are created within a fairly diffuse phase space, and even after ionization cooling the beam phase-space volume is relatively large. The acceleration system must accommodate that complete phase-space volume and compress it within the acceleration cycle to match the requirements of the collider. In this section we describe the constraints resulting from these requirements.

7.3 Lifetime Constraints

The muon lifetime is $\tau_\mu = 2.2\,\mu s$ in the muon rest frame. In the lab frame the lifetime is increased by the relativistic factor $\gamma = E_\mu/m_\mu$, where E_μ is the energy and m_μ is the mass ($m_\mu = 0.10566\,\text{MeV}$) of the muon. The muon decay rate along the beam path length s is

$$\frac{dN}{ds} = -\frac{1}{L_\mu \gamma}, \tag{7.1}$$

where $L_\mu = c\tau_\mu \approx 660\,\text{m}$, and where we have used the relativistic approximation $v/c \approx 1$. In a non-accelerating transport, this implies the usual exponential beam loss:

$$N = N_o e^{-\frac{s}{L_\mu \gamma}}. \tag{7.2}$$

In an accelerating section, γ is not constant:

$$\gamma = \gamma_o + \gamma' s = \gamma_o + \frac{eV'_{rf}}{m_\mu c^2} s, \tag{7.3}$$

where eV'_{rf} is the accelerating gradient. Using this in the decay equation we obtain the solution

$$N(s) = N_o \left(\frac{\gamma_o}{\gamma_o + \gamma' s}\right)^{\frac{1}{L_\mu \gamma'}} \qquad \text{or} \qquad \frac{N(s)}{N_o} = \left(\frac{E_o}{E_{\text{final}}}\right)^{\frac{1}{L_\mu \gamma'}} \tag{7.4}$$

where E_o and E_{final} are the initial and final energies within the accelerating section. Low losses require that the exponential factor must be small, which means that $L_\mu \gamma' >> 1$. This can be written as $L_\mu \frac{eV'_{rf}}{m_\mu c^2} >> 1$, which means $\mathbf{eV'_{rf} \gg 0.16}\,\text{MV/m}$ is required. This general rule must be followed throughout the entire muon system. For example, beam-cooling and reacceleration must also occur in systems whose averaged accelerating gradients (including loss and transport elements) are much greater than $0.16\,\text{MeV/m}$ to avoid large decay losses. For a multiturn muon accelerator, the gradient criterion can be rewritten as

$$E' \rightarrow \frac{E_{\text{final}}}{N_{\text{turns}} 2\pi R} \gg 0.16\,\text{MeV/m}, \tag{7.5}$$

where R can be written in terms of the mean bending field B of a complete turn at full energy and the magnetic rigidity $B\rho$ as $R = B\rho/B \approx 0.00334\,E_{\text{final}}(\text{MeV})/B(T)$, and N_{turns} is the total number of acceleration turns. Inserting this into the previous equation obtains a criterion for any multi-turn accelerator:

$$\frac{\mathbf{N_{\text{turns}}}}{\mathbf{B(T)}} \ll \mathbf{300}. \tag{7.6}$$

Thus, multiturn $\mu-$acceleration with up to hundreds of turns is possible. The gradient criterion requires somewhat faster acceleration than has typically been obtained in previous multi-pass systems, and that constrains our choices in acceleration systems (see below).

7.4   Phase Space and Intensity Constraints

The acceleration system must take beam from the cooling system to full energy. In the cooling section, the initial muons are collected, cooled, and pre-accelerated into moderately compact μ^+ and μ^- bunches at $E_\mu \approx 1\,\mathrm{GeV}$. Studies of the cooling system indicate that an rms energy spread of $\approx 1.5\,\%$ with a bunch length of $\approx 25\,\mathrm{cm}$ at $1\,\mathrm{GeV}$ are reasonable design goals, and we use these as reference initial parameters. The accelerator must accelerate these bunches to $2\,\mathrm{TeV}$ and transfer them into the collider, which requires a final energy spread of $\approx 0.1\,\%$ and a bunch length reduced to $\approx 0.3\,\mathrm{cm}$. These collision requirements set the longitudinal phase-space area of the beam at collisions at $\approx 3\,\mathrm{mm} \times 2\,\mathrm{GeV}$ ($\frac{\Delta E}{E} = 0.001$ for $2\,\mathrm{TeV}$), or $0.02\,\mathrm{eV}$-s, which is not much larger than the beam emittance at the beginning of the acceleration. The cooling system also reduces the normalized transverse emittance to a design value of $\epsilon_N \approx 0.25 \times 10^{-4}$ m-rad. The acceleration system must accelerate this beam to full energy while maintaining an emittance of $\epsilon_N < 0.5 \times 10^{-4}$ m-rad. Thus relatively little emittance dilution can be allowed in the acceleration and beam transfers, both transversely and longitudinally. Also transport dynamic and physical apertures must be sufficient to accept the beam throughout the accelerator, with low beam loss. The design intensity is 2×10^{12} μ's per bunch, which is a relatively high charge per bunch (larger than existing accelerators). The acceleration system must also accommodate these intense bunches. Wakefield and beam loading effects can become important, particularly in the higher-energy end of the accelerator, where bunch-lengths are reduced toward $0.3\,\mathrm{cm}$, obtaining high-peak currents. Another intensity-dependent limitation is μ-decay in the transport, which will deposit electrons with an average of $1/3$ of the μ energy throughout the system. Since the decay rate decreases as the energy increases, the mean beam energy deposition per meter and per μ is a constant

$$\frac{dE}{ds} = \frac{m_\mu c^2}{3 L_\mu} \quad (\text{per } \mu). \tag{7.7}$$

This comes to $\approx 0.5\,\mathrm{watts/m/turn}$ from a beam of 2×10^{12} μ's at $30\,\mathrm{Hz}$. This level could become a significant problem with multiturn passes through superconducting elements.

7.5   Acceleration Options

From these constraints, we can develop acceleration scenarios, which include full-energy linac, rapid-cycling synchrotron and recirculating-linac options, as well as hybrid approaches.

7.5.1   Single Pass Linac

A single-pass linac can easily meet the gradient constraint. For instance, the SLAC linac has a gradient of $17\,\mathrm{MV/m}$, roughly $100\times$ the gradient criterion. However single-pass rf structures are prohibitively expensive and do not exploit a primary advantage in muons: our ability to bend them into multipass devices, enabling multipass use of the accelerating structures. As discussed above, the μ lifetime is sufficiently long to permit multipass acceleration.

7.5.2   Recirculating Linacs

A multiturn approach is the use of recirculating linacs. A schematic view of a recirculating linac is shown in Fig.7.1. In a recirculating linac (RLA), the beam is accelerated and returned for several passes of acceleration in the same linac, but a separate return path is provided for each pass. At the end of the linac, the beam passes through beam-separation dipoles, which sort the beam by energy, directing it to an energy-matched return arc (A pulsed kicker magnet system may also be used for the beam separations). The various energy transports are then recombined at the end of the arc for further acceleration in the following linac. The beam passes through both arcs and linacs until full energy is reached, and the beam is then transferred from the highest energy line to the next RLA or the collider.

The RLA permits economic reuse of an expensive accelerating structure for several turns of acceleration. Since the beam passes through a separate transport on each turn, the magnets can be at fixed-field, allowing superconducting magnets, and simplified designs. However since each turn does require a separate return transport, cost and complexity considerations limit the number of turns to a finite number ($\approx 10 - 20$). This is very compatible with the lifetime constraint: $(N_{\mathrm{turns}} << 300B(T))$, which then can be met with relatively modest field magnets, and typically beam-decay survivals of $\approx 95\,\%$ are obtained in μ RLA's. High-field magnets are not required. RLA's are rather ideally matched to the μ lifetime constraint.

The same RLA system can be used to accelerate both μ^+ and μ^- bunches. The oppositely charged bunches would propagate around the RLA's in opposite directions. If the bunches are injected into opposite sides of each RLA at the beginning of the separate linacs, then energy match of the beams in each arc is obtained, as well as phase matching across the arcs. Separate (but symmetric) transport lines into the higher-energy RLA's and into the collider would be needed.

Because of the independence of each return transport, there is a broad flexibility in RLA design, with only the rf acceleration frequency and voltage remaining constant from linac pass to linac pass. Since return paths are independent, the synchronous phase ϕ_s and the chronicity, $M_{56} = \frac{\partial z}{\partial(\delta p/p)}$, where z is the particle position within the bunch, can
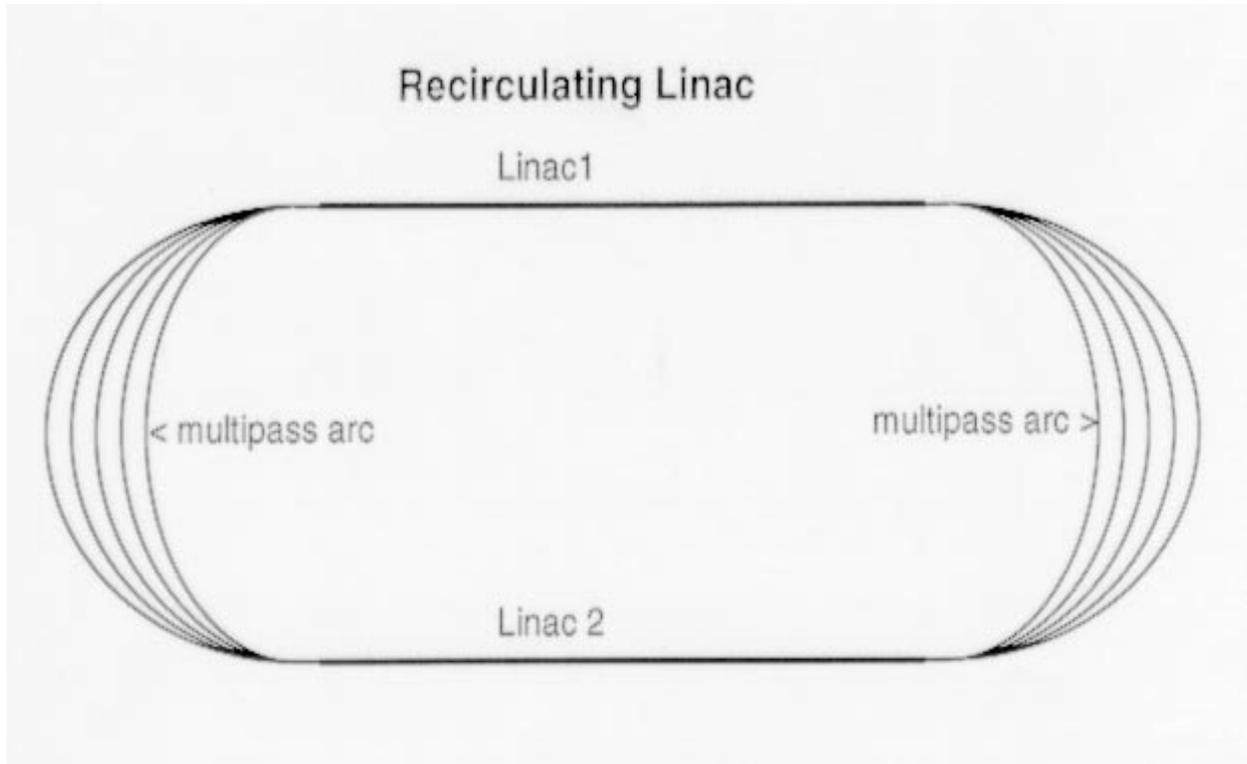
Figure 7.1: Schematic view of a recirculating linac (RLA). The beam is accelerated through several passes of the linacs. On each return arc, the beam passes through a different transport path, matched to the increasing beam energy. Magnetic fields are fixed and the number of return transports (per arc) equals the number of linac passes.

be changed arbitrarily from pass to pass to fit the beam-bunching requirements. Higher-harmonic rf and/or additional compressor arcs can also be added, if needed. (Our prototype RLA acceleration scenario does use a bunch length compressor at the beginning of each RLA.)

The major disadvantage in the RLA is the large cost associated with providing a separate transport for each return arc. Cost-saving transport systems or multi-pass design modifications are desired.

7.5.3   Rapid-Cycling Synchrotrons

A rapid-cycling synchrotron consists of rf accelerating structures within a circular magnetic beam transport, and the magnetic fields are increased from low-field to high-field while the beam is accelerated from low to high energies, passing many times through the same transport system. in Fig.7.2 The magnetic fields must change rapidly to follow the beam accel-

Rapid-Cycling Synchrotron

rf⎪   ⎪rf
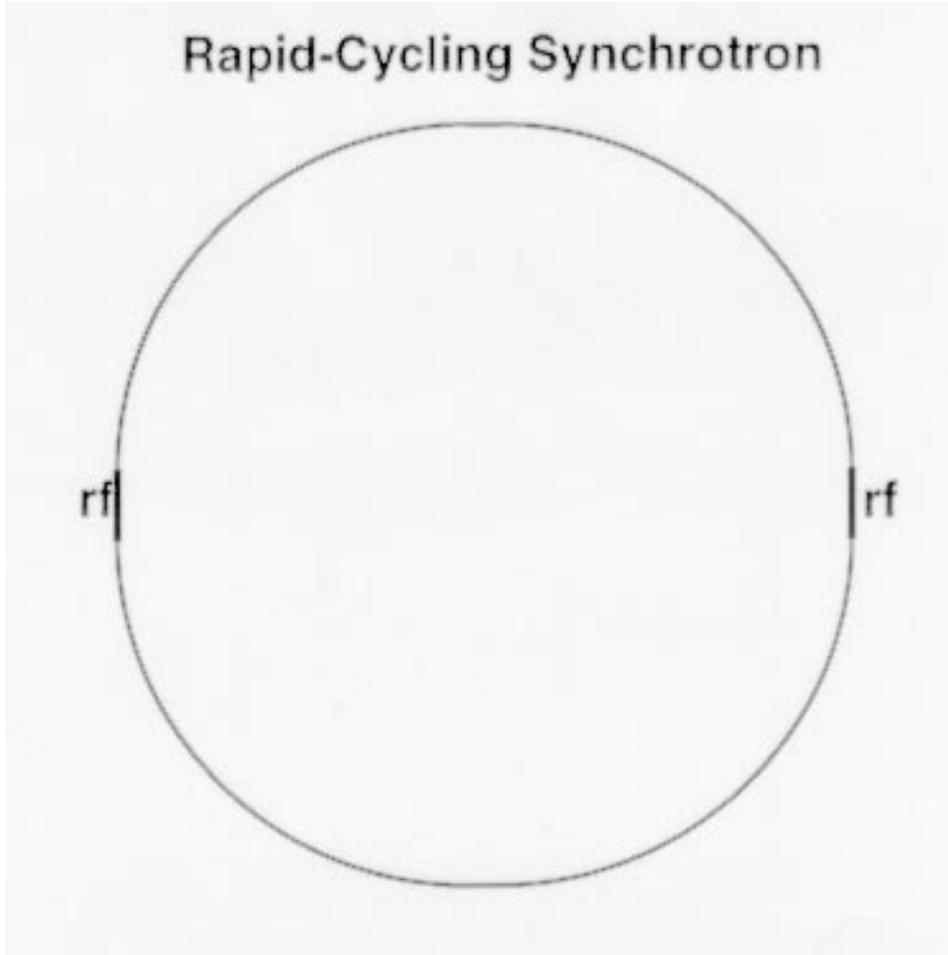
Figure 7.2: Schematic view of a rapid-cycling synchrotron (RCS). The beam is accelerated for many turns through the rf, while the magnetic fields in the ring cycle from low-field to high-field following the beam energy.

eration. In currently established technology, rapid-cycling synchrotrons use iron-dominated conventional magnets ($B < 2\,T$) and cycle at AC rates ($f < 60\,\mathrm{Hz}$). Only high-energy muons have sufficiently long lifetimes for these cycle times. As an example, the beam could be accelerated from 100 to 2000 GeV in a ring with $R = 5\,\mathrm{km}$ ($B = 1.33\,T$) using a 19 GV/turn rf system (1 km of 19 MV/m rf) in a 100-turn cycle, and this would have an acceleration cycle of $\approx 12\,\mathrm{ms}$ with a decay survival of 46.2 %. This would still be a large and rather expensive system. Higher-frequency cycling magnets could be developed, but would require very thin laminations (see below).

Instead of iron-dominated magnets, we are also investigating the recently-developed possibility of using pulsed conductor magnets, and these could cycle at much faster rates and reach higher fields than more established technology. These would more easily meet the

acceleration criterion ($N_{\text{turns}} \ll 300B(T)$), and could be used for lower energies. These are discussed in more detail below.

Other rapid-cycling scenarios, using such possibilities as transports containing both high-field and rapid- cycling elements, or obtaining rapid-cycling by rotating fixed-field magnets, are being developed, and are also discussed below. While a practical technology is not yet well established, rapid-cycling elements will probably be incorporated into an eventual μ-accelerator.

7.6 Acceleration Scenario

Within currently developed technology, recirculating linacs appear clearly possible, and are reasonably well matched to μ-accelerator requirements. We will therefore consider RLA acceleration in more detail. As a proof of principle, we present and discuss an explicit acceleration scenario for the 2 TeV collider.

7.6.1 Baseline Scenario Description

In this baseline scenario, the beams are accelerated from 1 GeV to full energy (2 TeV). In this process, the $\mu-$bunch lengths are compressed from $\approx 0.25\,\text{m}$ at 1 GeV to a length of $\approx 0.003\,\text{m}$ at full energy. It is also important to obtain the acceleration and bunch compression with minimal phase space dilution, in order to avoid energy-spread blowup and beam losses. These factors of a 1000 in energy increase and 100 in bunch-length compression are not practical in a single RLA. A sequence of RLA's, with rf frequency increasing as the bunch length decreases, are used. A schematic view of such a multi-stage RLA accelerator is displayed in Fig.7.3 and parameters for our initial prototype scenario are displayed in Tb. 7.1.

This scenario is a modularized 4-stage RLA system, with parameters based on discussions in the collaboration meetings. In each stage the energy is increased by a factor of < 10 (1 to 9 to 70 to 250 to 2000 GeV).[1] The rf frequency is also increased from RLA to RLA, from 100 to 350 to 800 to 1300 MHz, as the bunch length decreases. Each of the 4 RLA's consists of two linacs (with 0.5, 3, 8, and 56 GV of rf per linac for RLA 1, 2, 3, and 4, respectively) with recirculating arcs connecting them, and a total of $9 - 16$ turns in each stage. This prototype scenario also includes buncher rf and transport systems (B1, B2, B3, B4) at the entrance of each RLA. Most of the bunch-length compression occurs within the buncher systems, which use the same rf as the RLA acceleration systems but are much shorter.

We have simulated this initial scenario using the program μRLA, and some results are

Table 7.1: Parameters of a 4-RLA scenario

|	Buncher 1	RLA 1	Buncher 2	RLA 2	Buncher 3	RLA 3	Buncher 4	RLA 4
Energy in (GeV)	1	1	9.6	9.6	70	70	250	250
Energy out (GeV)	1	9.6	9.6	70	70	250	250	2000
Nturns		9		11		12		16
V_{rf} per linac (GV)	0.08	0.5	0.86	3	2.64	8	10	56
ϕ_s (degree)	90	20	90	15	90	16	90	14
rf frequency (MHz)	100	100	350	350	800	800	1300	1300
gradient (MV/m)	5	5	10	10	15	15	20	20
L(linac) (m)	16	100	86	300.0	176.0	533.3	500	2800
Arc length (m)		30		175		520		3500
B_{arc} (T)		3.4		4.2		5.2		6.0
M_{56} per arc (m)	6.0	$0.4 \rightarrow 1.9$	1.5	$0.1 \rightarrow 0.6$	1.5	$0.15 \rightarrow 0.6$	0.8	$0.3 \rightarrow 2.3$
Time in module (μs)		7.8		35		84.2		672
Decay Losses(%)		9.0		5.2		2.4		3.6
Bunch Length (cm)	$25 \rightarrow 8.3$	4.8	1.4	1.3	0.72	0.59	0.30	0.29
ΔE_{rms} (GeV)	0.05	0.09	0.31	0.34	0.61	0.80	1.5	1.5
Emittance (eV-ms)	13.6	14.0	14.0	14.1	14.0	15.1	15.0	14.2
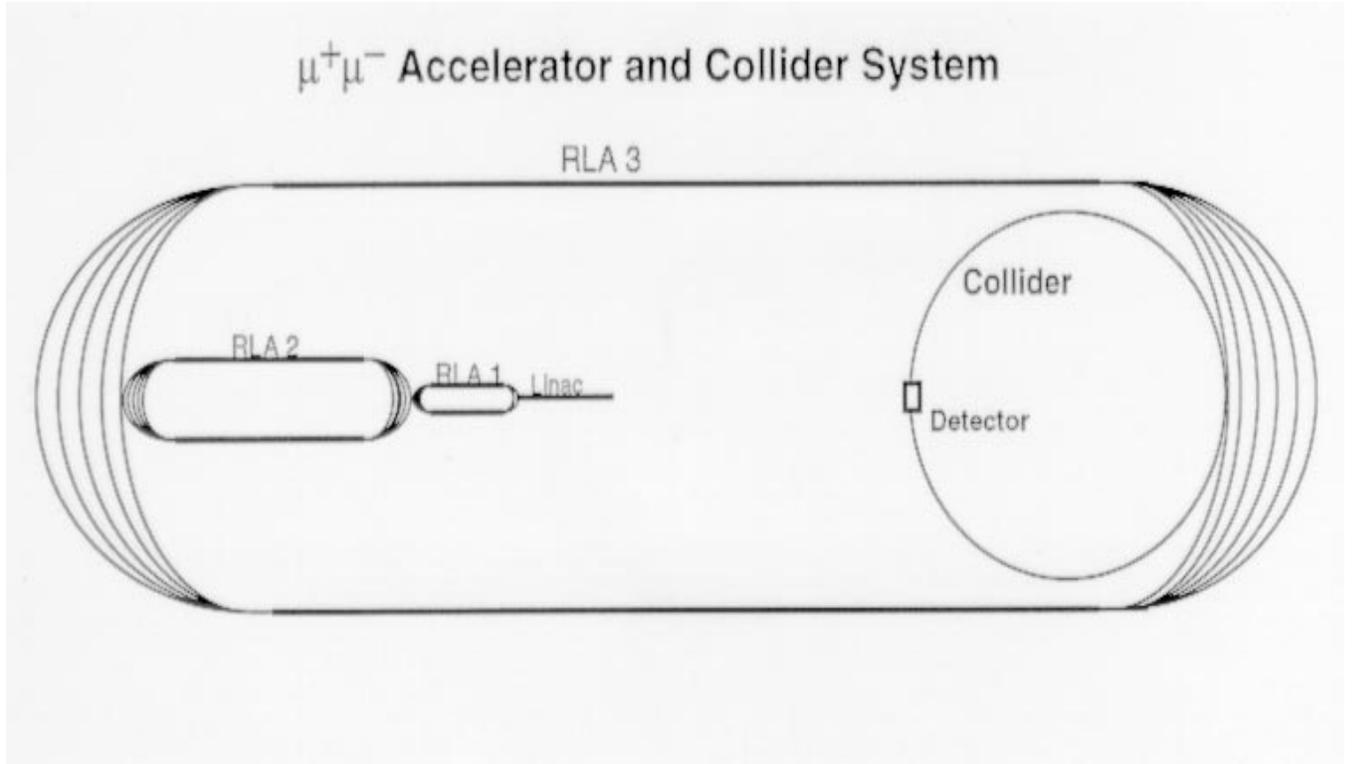
Figure 7.3: Conceptual view of an multi-stage RLA-based accelerator, showing a linac feeding beams into a sequence of 3 recirculating linacs (RLA1, RLA2, RLA3) followed by a collider ring. Note that the drawing is not to scale.

included in Tb. 7.1, and displayed in Fig.7.4. Some phase-space dilution and mismatch does occur, particularly in transfers between RLAs. However the rms emittance dilution is $< 5\,\%$ per RLA or $10\,\%$ over the entire system. Particle loss through the beam dynamics is less than $1\,\%$. Particle loss through μ-decay is somewhat larger, but less than $\approx 5\,\%$ per RLA or $\approx 20\,\%$ over the entire system. (We have assumed mean gradients of up to $20\,\mathrm{MV/m}$ in the linacs, and mean bending fields of up to $\approx 6\,T$ in the arcs.) Bunch compression to $\sigma < 0.003\,\mathrm{m}$ is obtained through rebunching and matching with the frequency increase from RLA to RLA, and is acceptable.

The simulations demonstrate that a cascade of RLAs can provide acceptable acceleration with bunching for a $\mu^+\mu^-$ collider, with minimal dynamic and decay beam loss and emittance dilution. This scenario sets a *proof of principle* baseline for the exploration of acceleration scenarios. It is certainly not fully optimized, and does not exploit the full degrees of freedom possible in RLA scenarios.
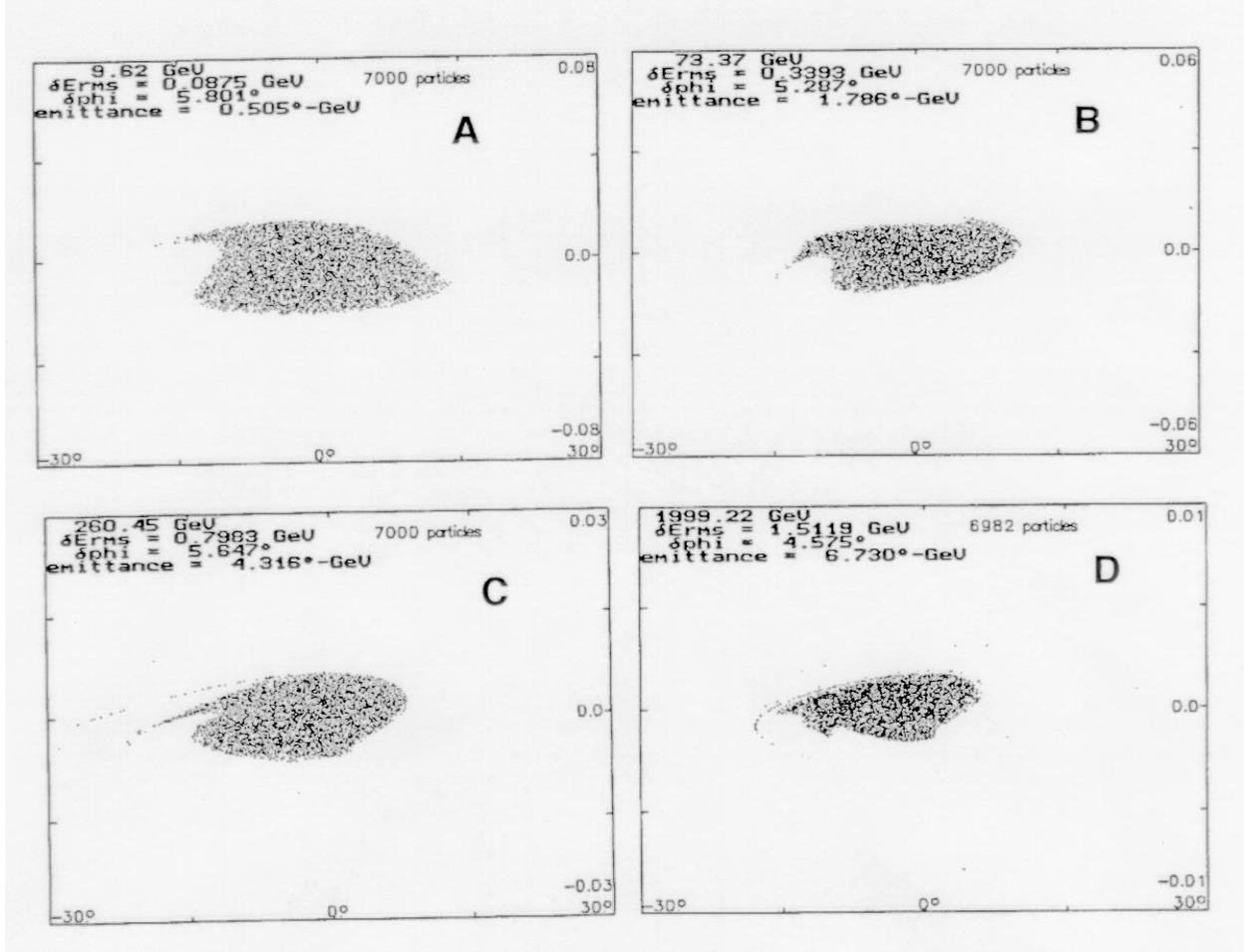
Figure 7.4: Some simulation results from the code μRLA.

7.6.2 Bunching/Acceleration Considerations

The acceleration and bunching must occur with minimal phase space dilution. The flexibility inherent in RLA scenarios permits many variations in compression scenarios, but it is also quite easy to obtain very badly matched schemes within that broad flexibility. Phase-space dilution can be avoided by careful phase-space matching of the beam in each stage of the acceleration scenario.

Within an RLA, phase space dilution can be minimized by matching the bunch in both energy and phase to the stability region or "rf bucket" associated with the longitudinal motion parameters. That defines a region in phase space that extends in phase from $-\phi_s$ to $\approx 2\phi_s$, where ϕ_s is the stable acceleration phase, and in energy spread to

$$\frac{\Delta E}{E} = \pm\sqrt{\frac{eV_{rf}\lambda}{EM_{56}}}\sqrt{\frac{2(\sin\phi_s - \phi_s\cos\phi_s)}{\pi}} \approx \pm\sqrt{\frac{2eV_{rf}\lambda}{3\pi EM_{56}}}\phi_s^3 \tag{7.8}$$

where V_{rf}, λ are the rf voltage (per linac) and wavelength, and M_{56} is the chronicity of an arc:

$M_{56} = \frac{dz}{d(\Delta E/E)}$, where $z = \frac{\lambda\phi}{2\pi}$. Efficient acceleration requires keeping the phase ϕ_s as close to crest ($0°$) as possible. Minimal nonlinear acceleration spread also requires minimal bunch length. In initial scenarios, we have minimized phase-space dilution by minimizing bunch lengths within the RLA and maintaining matched energy spread using the above equation. For fixed ϕ_s this implies that ΔE should remain constant, which implies that M_{56} should increase linearly with energy E. (A similar condition occurs naturally in microtrons.)

Bunch-length compression with minimal phase space dilution is obtained through a separate buncher system in which the beam passes through an rf system at zero crossing ($\phi_s = -90°$) followed by a compressor arc. At zero crossing, the nonlinear content of the rf acceleration is minimized and a very long bunch (up to $\Delta\phi = \pm60°$) can be compressed with minimal distortion.

Thus in our initial scenario, we have chosen a separated-function approach in which most of the bunching occurs in bunchers at the beginning of each RLA, and bunch-lengths are kept nearly constant within the body of the RLA. This separation minimizes nonlinear acceleration and consequent phase-space dilution. This requires a separate rf system for bunching at the entrance of each RLA (see Tb. 7.1); however these systems are a small fraction of the acceleration rf, and these separate rf systems are possible.

However, this separated function approach is not required, but is an initial simplifying approximation for this first proof of principle example. Modification of phase and M_{56} in the last and first few acceleration half-turns of each RLA can provide the same bunching effect. In future scenario development, the bunchers will be more integrated with the acceleration rf, reducing the need for separate systems and enabling more gradual bunching.

7.6.3   Injector and Matching from Cooling

For injection, we have used idealized $\approx 1\,\mathrm{GeV}$ beams with an energy spread and bunch length within reasonable reach of ionization cooling systems. However we do not yet have complete conditions for matching from the cooling system. An initial acceleration and matching system is needed to take the beam from the low-energy of final cooling energy-loss into the RLA system. This will be an $\approx 1\,\mathrm{GeV}$ low- frequency linac, with initial bunching, and parameters for such a system are described in Tb.7.2.

Beam production and cooling studies should more precisely define the μ-source, which in turn will specify the injector linac requirements, and the revised matching conditions may affect the initial specifications of the RLA system.

Table 7.2: Injection Linac parameters

Energy in	(GeV)	0.10
Energy out	(GeV)	1.0
Bunch length in	(m)	1.0
Bunch length out	(m)	0.25
ΔE_{rms} in	(MeV)	5
ΔE_{rms} out	(MeV)	20
frequency	(MHz)	$30 - 100$
Linac length	(m)	200
decay losses	(%)	8

7.6.4   Scenario Variations

In this baseline design, we have used a 4-RLA system. There is considerable variation allowable in the multiple-RLA concept, and we have previously presented other 3- and 4-RLA designs. The initial and final energies of each RLA, the number of passes, and the rf frequency in each RLA can be changed. In Ref.[2] we described a 3-RLA scenario with 2 to 20 to 200 to 2000 GeV acceleration using 100, 400 and 1600 MHz rf. and in Ref.[3] we also developed a 4-RLA scenario (1 to 9.6 to 80 to 250 to 2000 GeV using 100, 400, 1300 and 2000 MHz). In general, using fewer RLA's and fewer passes simplifies matching and reduces decay losses but increases rf requirements. Phase space acceptance into lower-frequency rf is also somewhat easier. In the present example we have chosen 4-RLA's with frequencies of 100, 350, 800, and 1300 MHz. The 250 GeV end-point of the third RLA is chosen to match a possible energy for a first-stage demonstration collider (250×250 GeV). The rf frequencies of 350, 800 and 1300 MHz are chosen because they match existing and planned SRF systems at CERN (350), LANL (800), and DESY/TESLA (1300). This allows the direct extension of previous experience to this new application, possibly even using some of the same components. In particular, the intensive SRF **R&D** effort at DESY has goals which are very close to our requirements (high gradient, high power, moderate cost, etc.) and could result in large SRF systems that can be adapted to our accelerator, and we have used this frequency for most of our acceleration. The peak frequency of 1300 MHz is also compatible with our high-intensity constraints. Wakefields at the DESY/TESLA level appear tolerable (see below), and a higher SRF frequency should obtain larger wake-fields. In this first scenario, we have used separate bunching rf and transports between RLA's.

This is not entirely necessary, and much of the bunching can be incorporated in the final and initial passes of the RLA's, by changing ϕ_s and M_{56} in those passes. For example, we have found a variant solution with similar performance, in which the bunching at 250 GeV between RLA's 3 and 4 is incorporated into a last half- pass of 3-RLA and the first full pass of 4-RLA. This more gradual bunching also reduces the peak relative energy spreads ($\Delta E/E$) in the initial RLA passes. Multi-harmonic rf systems could also be used to improve linearity, particularly in bunching, but have also not been included in this first scenario.

7.7 Acceleration System Components

In a multiturn RLA system there is a balance between rf acceleration and beam transport costs and requirements. Increasing the number of turns per RLA directly reduces the linac lengths and therefore linac costs, but it also increases the total amount of beam transport, adding cost and complexity. We have not yet developed sufficiently detailed cost estimates that can determine an accurate optimum. In this section we discuss some of the considerations which must be included in developing an optimum design.

7.7.1 rf Considerations

We need a separate rf linac system for each RLA, with lower frequencies for the initial lower-energy RLAs, where the beam has a relatively long bunch length, and higher frequencies for the high energy end, where the bunches are shortened. Very high-gradient is not essential in the acceleration, but rather minimal cost is. The Tb. 7.1 scenario requires ≈ 150 GV of rf cavities; this would require ≈ 7.5 km of accelerating structures at 20 MV/m. This includes $3 - 4$ separate rf systems, which we have labeled as low frequency (≈ 100 MHz), medium frequency ($300 - 800$ MHz) and high frequency ($1300 - 2000$ MHz) systems. We will discuss the various requirements of these sections next.

Low-frequency (≈ 100 MHz)

The first RLA in our scenario uses 100 MHz rf to accelerate beam from ≈ 1 to 9.6 GeV using two 0.5 GeV Linacs in a 9-turn cycle. Tb.7.3 shows parameters for the 100 MHz rf system and Fig.7.5a shows possible cavity cross-sections, with field lines.[4, 5] The 100 MHz cavities are designed to provide an average accelerating gradient of ≈ 5 MV/m through the linac channel.

In order to achieve this gradient, peak surface fields within the cavity will be 18 MV/m while the cavity-to-cavity displacement along the linac line will be 120 cm. The cavities will

Table 7.3: rf parameters for 100, 350, 800 and 1300 MHz systems

Frequency (MHz)	100	350	800	1300
rf type	Cu 300K	4.5K SRF	2K SRF	2K SRF
Cavity Design Source	FNAL-BNL	CERN	LANL	DESY
Cells/cavity	3	4	7	9
Cavity active length 9cm)	3×90	170	127.2	103.5
Cavity total length (cm)	360	240	186	135
Cavity beam aperture (cm)	22.5	37.7	17	10.3
cavity outer radius (cm)	90	37.7	17	10.3
Q	54000	3.2×10^9	3×10^9	3×10^9
Peak field/accel. field	3.6	2.1	2.09	2.0
Average design gradient (MV/m)	5	10	15	20
Reference gradient (MV/m)	5	6	12.5	25
rf peak power (MW)	3×1.9	0.1	0.15	0.21

run at an rf power level corresponding to 1.9 Kilpatrick limit, which is not excessive for this pulsed rf system. The peak and average rf power characteristics (see Tb.7.3) are well within capabilities of standard rf sources. The cavity has a fill ratio of 33 % for the gap length to linac length. This allows additional components to be installed along the beam line such as focusing elements, beam monitoring devices, etc. $100\,m$ of linac will be necessary in order to achieve an acceleration of $500\,\text{MeV}$. This will require a total rf power consumption rate of $360\,\text{KW}$.

Medium-frequency ($\approx 300 - 800\,\text{MHz}$)

In our scenario, we have used $350\,\text{MHz}$ rf in our second RLA. This RLA accelerates beam from 9.6 to $70\,\text{GeV}$ in 11 turns and requires two $3\,\text{GeV}$ linacs. The rf system must be active for $\approx 40\,\text{ms}$ at $30\,\text{Hz}$ in the present scenario (0.12 % duty cycle). While it is not certain that these must be superconducting, the frequency is quite close to the CERN LEP II SRF system ($350\,\text{MHz}$), [6, 7, 8] which operates at $6\,\text{MV/m}$ with high cw currents. That technology could be adapted to our application. We need $6\,\text{GV}$ of $350\,\text{MHz}$ acceleration in the present scenario, and this is roughly three times that installed in CERN LEP II. It is reasonable that improvements (such as adding high-power pulsed processing) plus low-

duty cycle operation would permit gradients of $10 \, \text{MV/m}$ or (hopefully) more. Experimental studies are under consideration to determine the effectiveness of pulsed operation and of pulsed power processing in these cavities.
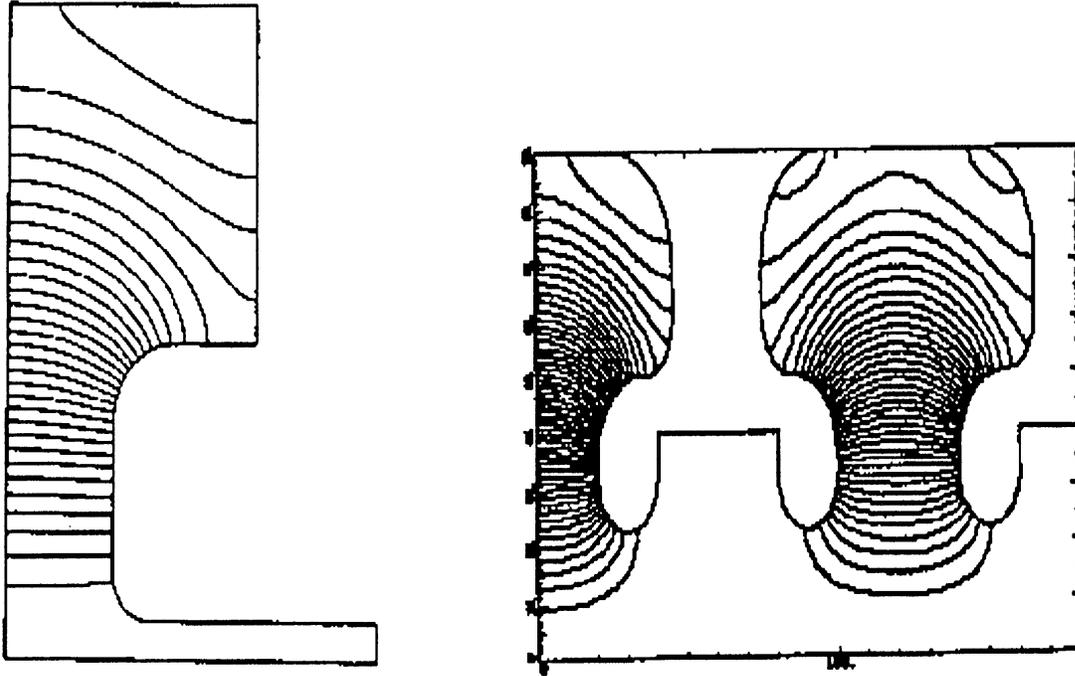

Figure 7.5: $100 \, \text{MHz}$ rf cavity systems with field lines. Figure shows half of a single cell cavity and half of a 3-cell cavity.

We have used $10 \, \text{MV/m}$ in the present scenario. Fig.7.6 shows a cross-section of CERN $350 \, \text{MHz}$ SRF cavities. These cavities are made of copper with a $1 \, \mu$ inner layer of niobium, which is magnetron sputtered on the interior. The copper provides good electrical and thermal conductivity for the bulk of the cavity while the niobium layer provided the superconducting cavity surface. Solid niobium cavities were also built; niobium-sputtered copper cavities were preferred because of better thermal stability, lower surface resistance, reduced external magnetic- field effects, and lower cost.

The present scenario uses $800 \, \text{MHz}$ rf in the third RLA (An alternative scenario using $1300 \, \text{MHz}$ has also been developed.). This RLA accelerates from 70 to $250 \, \text{GeV}$ in 12 turns, and requires two $8 \, \text{GeV}$ linacs. The rf system must be active for $\approx 100 \, \text{ms}$ ($0.3 \, \%$ duty cycle). The choice of 800 MHz is based on Los Alamos experience with $800 \, \text{MHz}$ SRF; $800 \, \text{MHz}$ was the PILAC design frequency.[9] The Los Alamos APT program also plans to develop SRF systems at $800 \, \text{MHz}$, and it is likely that the technology will be adaptable to high-gradient μ-
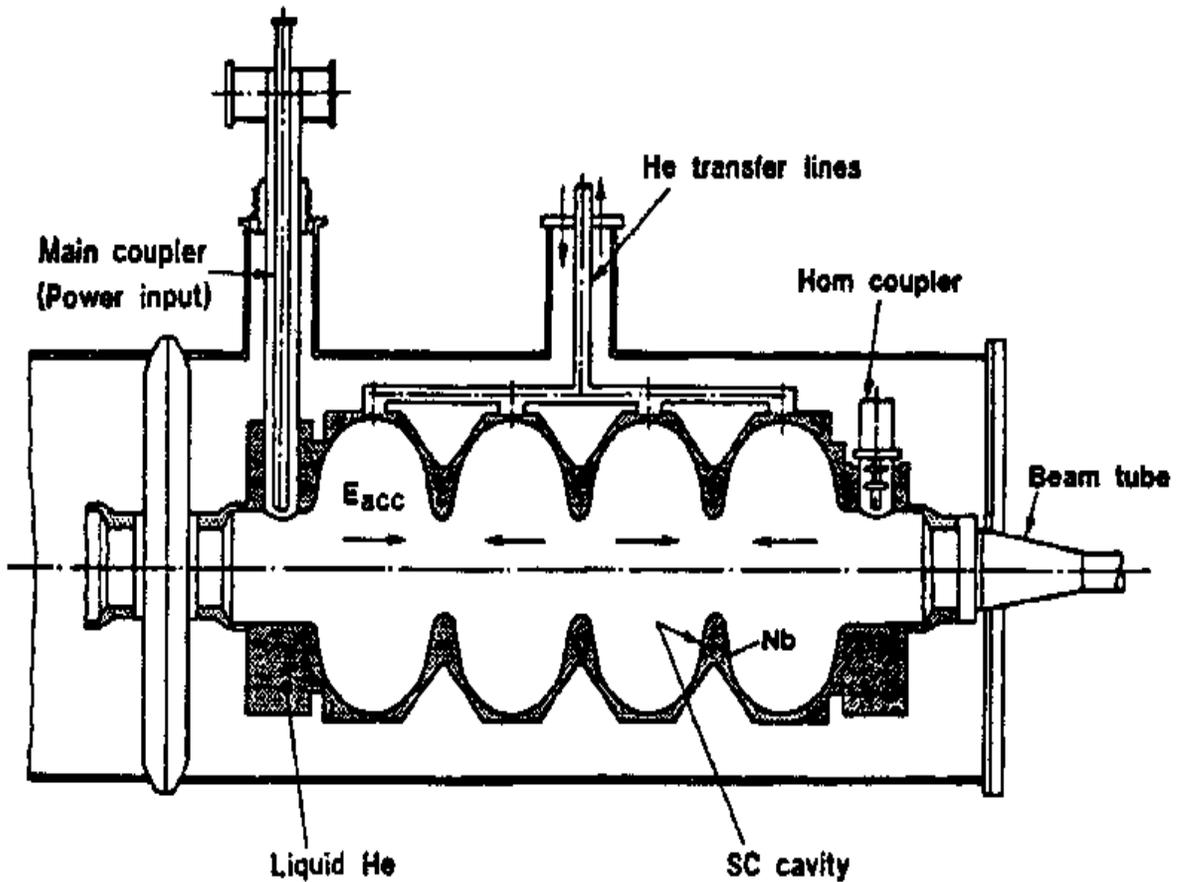
Figure 7.6: 350 MHz rf cavity system. Cross section of the superconducting CERN cavity.

acceleration, and could be included in our scenario. From Los Alamos experience a gradient of 20 MV/m seems possible,[10] and we have used 15 MV/m in Tb. 7.1. PILAC was designed for 12.5MV/mand 16MV/m was achieved. An advantage of 800 MHz systems are that they are (approximately) the highest frequency Nb rf systems that can operate at 4K liquid He temperatures, which simplifies cryogenic requirements and improves efficiency.

High-frequency ($\approx 1300 - 2000$ MHz)

In the present scenario, a 1300 MHz accelerator is used for the $250 - 2000$ GeV RLA. (We have also considered 2000 MHz for the $250 - 2000$ GeV RLA.) The accelerator uses two 56 GV linacs to accelerate beam to full energy in 16 turns. For economy, we require high gradient (≈ 25 MV/m) acceleration and the rf cavities must sustain field throughout the multipass acceleration time, which is 0.8 ms in the 2 TeV RLA, which implies a 2.4 % duty cycle. This is the largest acceleration system and it dominates the total SRF requirements.

The parameters imply that SRF cavities should be used, and SRF technology does promise high-gradient at these duty cycles. The TESLA SRF is designed at parameters extremely close to ours: up to $25\,\mathrm{MV/m}$ gradient at $1300\,\mathrm{MHz}$, active for $1\,\mathrm{ms}$ cycles repeating at $5-15\,\mathrm{Hz}$,[11, 12] and we plan to extend the results of that **R& D** effort to obtain the SRF system for our main acceleration system.

The TESLA SRF cavity is a 9-cell 1300MHz structure and is displayed in Fig.7.7.
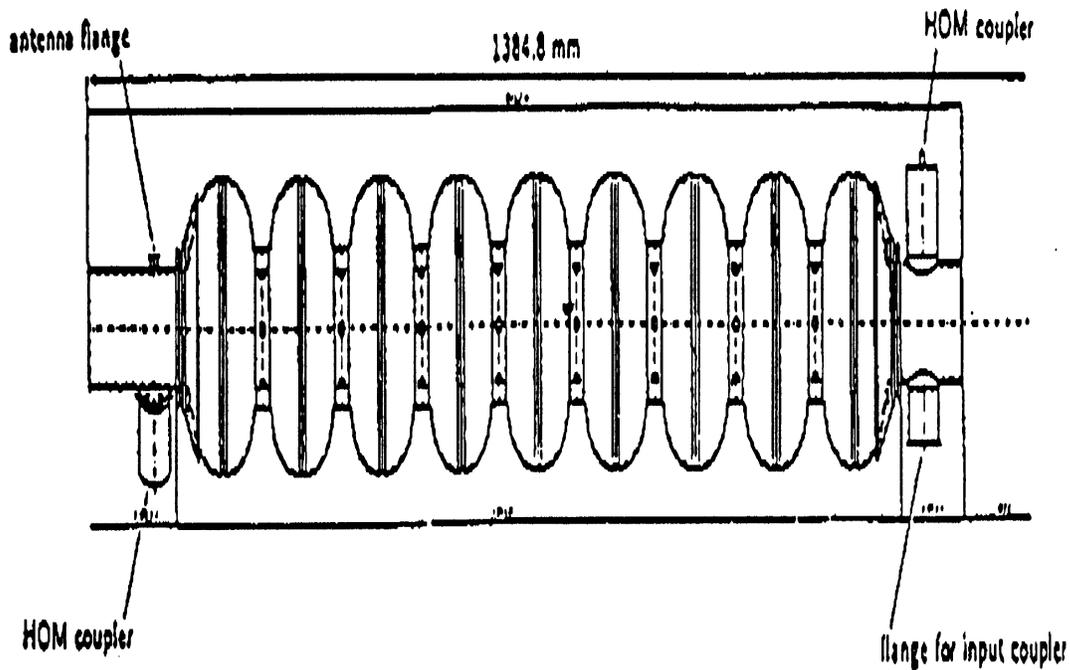
Figure 7.7: A TESLA 9 cell $1300\,\mathrm{MHz}$ cavity.

These cavities are made of high purity niobium sheets (2.8 mm thick) by standard fabrication methods (deep drawing and electron beam welding). It is critical in the cavity shape design to minimize the ratio of the peak to accelerating electric fields E_{peak}/E_{acc} (2) and the ratio of peak magnetic field to accelerating field H_{peak}/E_{acc} (4.2 MT/MV/m). The number of cells per cavity was limited to 9 because of higher order mode (HOM) damping requirements. There are one input power coupler and two HOM couplers (with $Q_{ext} = 10^4 \quad 10^5$) per cavity.

Because of the higher peak currents the HOM power requirements should be significantly larger in our application than in the TESLA case, so the couplers would need to be modified to handle the higher power. However, because the bunches are more widely spaced, the HOM damping rate need not be increased.

A TESLA cryomodule consists of 8 SRF cavities (a cost-effective choice) and is 12.2 m long. The total rf heat load to 2K in a cryomodule is estimated to be 21.4 W. The static heat load budget is 2.8 W at 2K, 14 W at 4.5K and 77 W at 70 K. We may need some additional cryogenic capacity to handle heating from muon decay products, although most of the electrons from decay will simply continue through to the end of the linac. HOM load cryogenics will also be modified. Magnetic shielding is included to improve cavity Q and the shielding reduces the residual external magnet field to less than 20 mgauss. 4 cryomodules (50m) share a klystron with 10 MW peak-power.

To obtain the highest possible gradients and cavity quality factors (Q), the TESLA **R&D** program is exploring methods to reduce and eliminate field emission (FE) and thermal breakdown in TESLA cavities. Key technologies which they are studying include : 1) Semiconductor industry standard cleaning techniques to remove FE particles from the rf surfaces, 2) Material removal from the cavity surfaces by chemical etching, 3) Increasing the thermal conductivity by employing Ti solid-state gettering in a pre-purification treatment in a ultra-high vacuum oven, 4) Rinsing cavities with high pressure deionized water to remove surface particles, 5)high-power rf pulse processing to remove the remaining FE sites. Significant progress has been made in these efforts: A recent prototype cavity has reached $E_{acc} = 26$MV/m with $Q = 3 \times 10^{10}$ in CW operation and $E_{acc} = 31$MV/m in pulsed operation.

In other scenarios, we have also considered $1600\,$MHz and $2000\,$MHz SRF systems for the final μ-accelerator, and these frequencies could be used in a final configuration. However we expect wakefield limitations to be worse for higher frequencies (see below). Also we expect that the intensive research in $1300\,$MHz cavities for TESLA will produce optimal high-gradient configurations which can be extended to our case, and therefore minimize the subsequent **R&D** requirements. [13]

Wake-field Considerations

A high-luminosity $\mu^+\mu^-$ collider will have very high-density bunches, with 10^{12} or more particles per bunch. At these high-intensities, collective effects can be important. In the short bunches prepared for the collider, the dominant effect is expected to be the short-range wakefield.

Mosnier and Napoly[14] have evaluated wakefields in the TESLA 9-cell structure (1300 MHz, $1\,m$ length), which is designed to accelerate at $25\,\mathrm{MV/m}$ and is thus very similar to the rf system for the high-energy high-frequency RLA(s). They obtain a maximum wakefield across an electron bunch of $1\,\mathrm{mm}$ length of $\approx 15\,\mathrm{V/pC}$. For $10^{12}\,\mu$'s ($1.6 \times 10^5\,\mathrm{pC}$), this is 2.4 MV or almost 10% of the accelerating voltage. Our bunches are 4 times longer than 1mm, and the short-range longitudinal wakefield is reduced in proportion to the square root of that length, so the wakefield would be a factor of 2 smaller. The wakefield is also proportional to $1/a^2$, where a is the cavity aperture. This aperture is naturally larger for longer wavelength (lower frequency) rf. The TESLA cavity aperture could be somewhat increased, by up to a factor of ≈ 2 to reduced wake-fields, but with some degradation of other cavity parameters. We may also have more than $10^{12}\,\mu$'s per bunch for high luminosity, and scenarios with up to 4×10^{12} have been generated. For our recirculating linac scenarios, we expect that the largest wake-field effects will occur in the highest- energy (2 TeV) recirculating linac, since that linac has the highest frequency rf and the shortest bunches. We have studied these effects by simulations of particle motion which include wake-fields in the final 200 to 2000 GeV linac of the 3RLA scenario of ref. 3. To include wakefield nonlinearity effects in our simulations, we have used a simplified short-range model in which the longitudinal wakefield deceleration on each particle is proportional to the charge in front of the particle, with the full bunch charge giving the total wakefield. (This model was used in the CEBAF FEL design. [15]) Following the TESLA values (scaled to 4mm bunch length) we estimate a total wakefield of 7.5 V/pC, or 1.2 to 4.8 MV wakefield per 25 MV acceleration for $1-4 \times 10^{12}\,\mu$'s. The first-order and second-order wakefield effects (magnitude and slope) can be compensated by increasing the rf voltage and changing the accelerating phase. Higher order effects are not compensated, and can give nonlinear distortion to the motion, causing emittance dilution and eventual beam loss. Some simulation results are displayed in Tb.7.4 and in Fig.7.8. For 1.0 and 2.5 MV (per 25 MV) cases we can increase the rf voltage (by 4% and 12.4%, respectively) and shift the rf phases from $12°$ at zero wakefield to $18°$ and $25°$, respectively. We then obtain similar performance to the zero wakefield case, with similar distortion and phase space dilution. For 5 MV, the rf voltage would need to be increased by 30% and the rf phase ϕ_ss moved to $35°$. Significant orbit distortion is seen (emittance dilution of 30%). Although no beam loss occurs, the phase space distortion is at the limit of acceptability. Thus for moderate size bunches ($1-2 \times 10^{12}$) the wake-fields can be compensated, but much larger charges could lead to significant distortion and beam loss. In further studies, it has also been found that the wake-field effects are reduced as the number of acceleration turns increases, since the beam develops more synchrotron oscillations which average the effects over the beam.

Table 7.4: μRLA simulation results with wakefields for a 2 TeV recirculating linac. In these simulations we used initially Gaussian beams with 20 eV-ms normalized rms emittance at 200 GeV.

Case	Wakefield amplitude	Accelerating rf voltage phase	Bunch depression	$\delta E_{\rm rms}$ Length(GeV)	Final Emittance
1	0	13°	0%	5.58°	2.41	22.5 eV-ms
2	1 MV/m	18°	4.5%	4.89°	2.68	22.0
3	2.5	25°	12%	6.06°	2.17	21.6
4	5	35°	26%	6.66°	2.71	31.3

In summary, the μ-collider design intensities are close to the intensities at which wake-field effects can become a limitation. Significant monitoring of the effects and accurate evaluations of the wake-fields are needed; it is important to ensure that the adverse effects are truly minimized.

7.7.2   Transport Considerations

The beam transports for the recirculation arcs are relatively straightforward, but are nontrivial, since they require good transverse matching throughout the system to avoid emittance dilution. High field is not required, and even conventional fields (B< 2T) can be adequate. Since the beam passes through a different return arc on each turn, the total amount of beam transport is relatively large (≈ 160 km of arcs in the baseline scenario). The transport can easily become very expensive, so cost-saving designs are needed, such as multiple-aperture or rapid-cycling hybrid designs, and these are presented below.

Transport lattices

Each transport must be achromatic (matched to zero dispersion), and also must have a chronicity M_{56} matched to the bunching requirements. A transport modeled on the CEBAF RLA could be used. The M_{56} values are small compared to the natural chronicities. The average dispersion in an arc (given by $\eta = M_{56}/\pi$) varies from ≈ 0.1 to 1 m in these cases. Flexible momentum compaction lattices, where the average η is reduced by including perturbations to negative η, could be used for some of these arcs.[16] Note that at the beginning and end of the arcs beam-separation and beam-recombination transports for all passes must be inserted, and this adds considerable complication. CEBAF[17] has a 5-pass
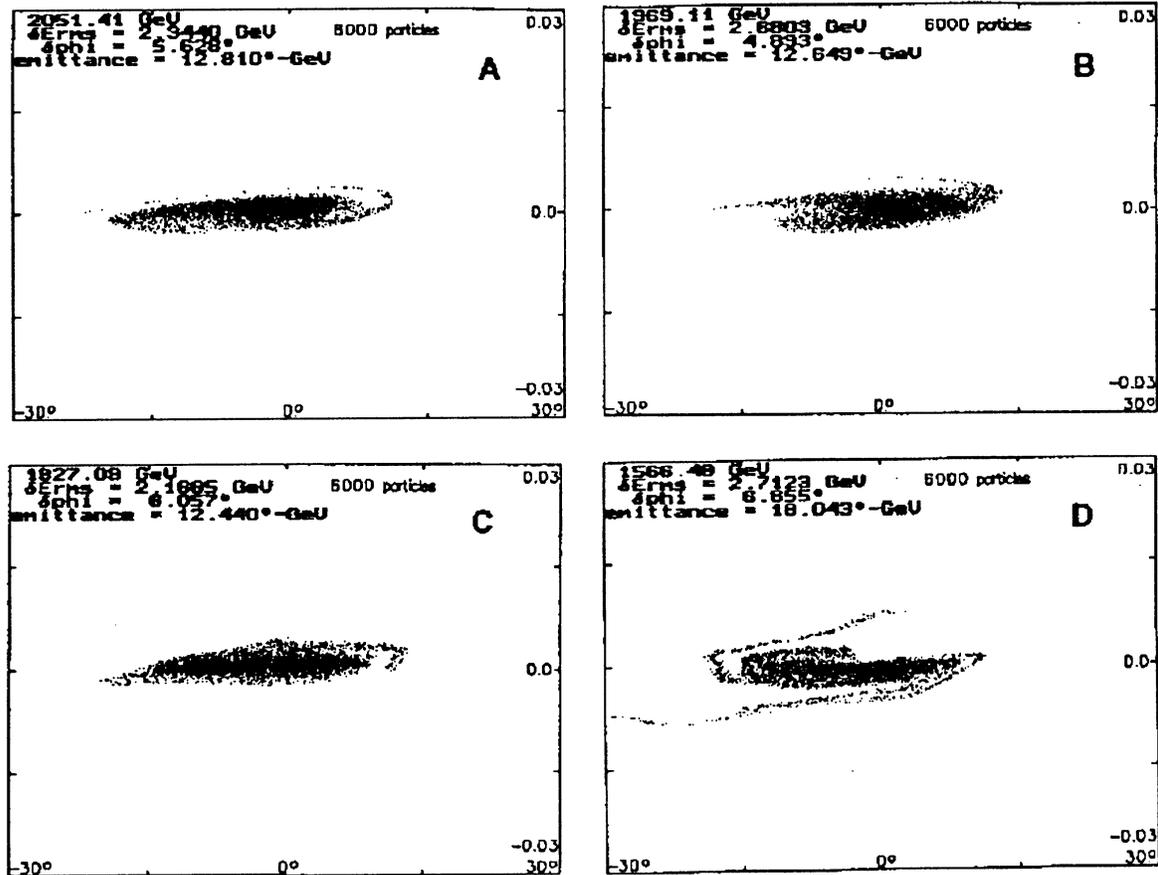
Figure 7.8: μRLA simulation results with wake fields, with beam accelerated from 200 to 2000 GeV in a 10-turn RLA.

separation and recombination system with carefully matched transports, and it is easy to imagine an $\approx$ 10-pass extrapolation of that system to our case, and that is what we have used. However many more passes (> 20?) may lead to impractically congested designs.

A significant concern is the relatively large energy spreads (up to 5% rms) which occur in the initial turns of the lower energy RLA's. Detailed design of arc transports which can accommodate these, without losses or emittance dilution, is a challenge. It is likely that the scenarios should be modified to reduce the energy spread requirements, possibly by keeping the bunches longer, which may require lower-frequency or multi-harmonic rf systems.

Recirculating Arc Magnets

Each recirculating linac (RLA) has two long, parallel linacs with a large energy gain per pass, and semi-circular arcs of fixed-field superconducting magnets at each end. Fig.7.9 is a

sketch of a RLA, showing the two arcs and two linacs and, enlarged, the separation, phasing, and steering magnets which direct the muons between the linacs and the recirculating arcs.
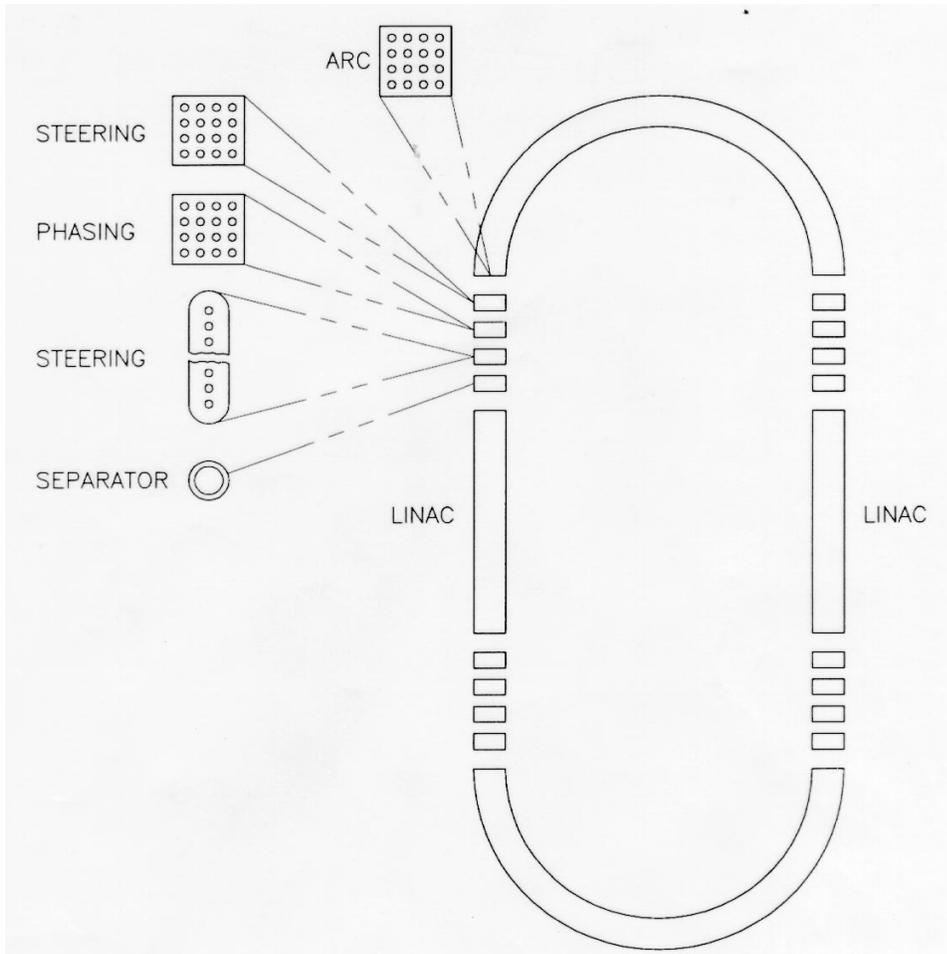
Figure 7.9: Overview of a μ recirculating linac, showing the arcs with beam separation and multiple-aperture magnetic transport.

The number of turns in each RLA depends upon a balance among cost, complexity and performance considerations of rf and beam transport components. These considerations may require as many as 20 recirculating passes; we present a magnet design for 16-passes in the highest energy RLA, corresponding to the current acceleration scenario. We use a multiple-aperture magnet design, in which the passes go through separate (different field) apertures in the magnetic structure.[18]

The design is presented in Fig.7.10, which displays a cross-section of a set of four stacked magnets, each containing 4 apertures, all within the same pressure vessel (cryomodule). The aperture at the top left has a field of 7 T, and there is an 0.406 T difference between adjacent apertures in a stack. With superconducting cable at SSC parameters, two layers of cable are
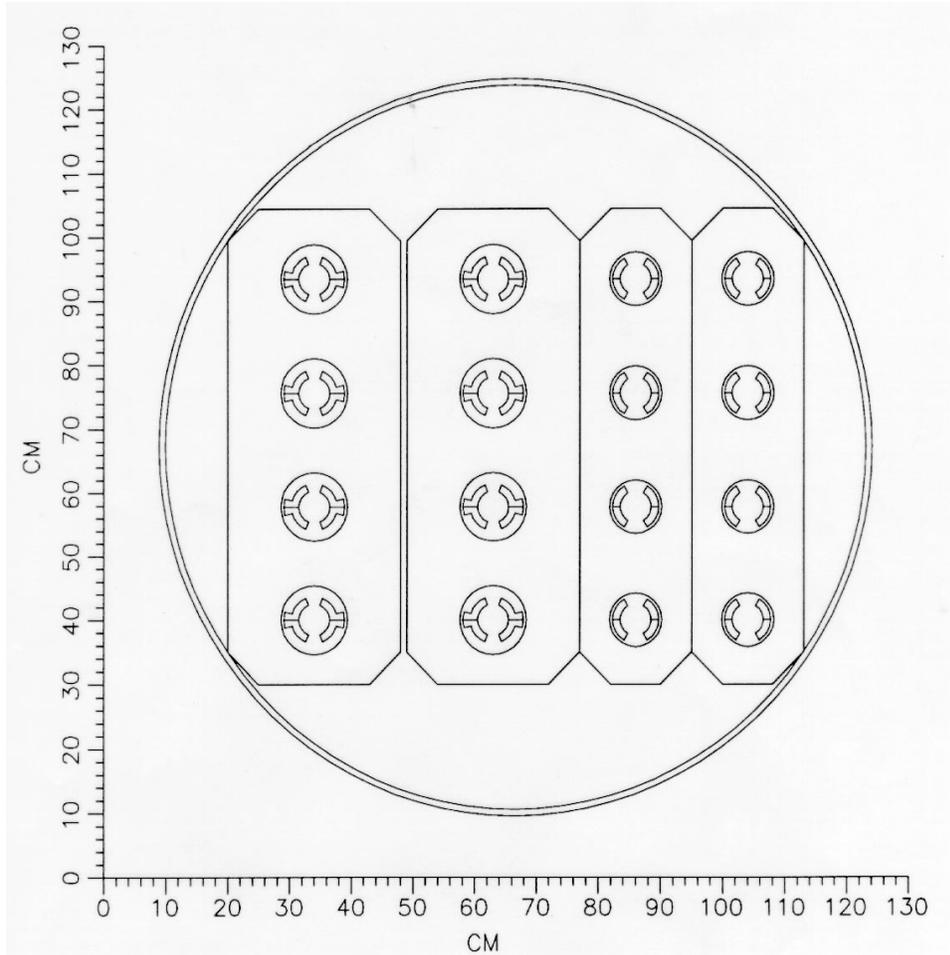
Figure 7.10: A 16-aperture dipole, composed of four stacks of four apertures. The highest field (7 T) aperture would be in the lower corner.

required for fields above ≈ 4 T, and we have arranged that all apertures in a stack have the same configuration. Thus there are 8 apertures with two-layer coils and 8 with single-layer coils. The two-layer coils eliminate sextupole and decapole components; the single-layer coils eliminate sextupole components. The two high-field stacks have two layers of superconductor in the apertures, each 12 mm thick. The highest current density is $31,000\,\mathrm{A/cm^2}$ in the 60 coils of the 7 T aperture (similar to the $29,000\,\mathrm{A/cm^2}$ in the inner layer of the 6.6 T SSC dipole). The lower currents for the lower field apertures would be obtained by using fewer turns.

The stacks in Fig.7.10 result in reduced reluctance for the flux return path (compared to individual magnets), thus reducing the amp-turn requirement in each aperture. However the stack arrangement would naturally have a vertical (skew) gradient in the field. This is eliminated by putting different currents in the upper and lower coils in an aperture. There

is also sufficient flux leakage out of the highest field stack to influence the field in the stack adjacent to it. However, the field in the space between these stacks is low enough that a thin foil layer of pure Nb, which has an H_c of $\approx 1.4 \times 10^5$ A/m (1800 Oe), could be used as an inexpensive shield, eliminating the flux leakage.

In this design, the pressure vessel also serves to constrain the transverse forces on the iron, which include the Lorentz force and the coil pre-stress forces. The wall of the pressure vessel could easily contain the assumed 20 atmosphere He pressure. However, the end plates must withstand Lorentz force on the coil ends and the He pressure, and must have penetrations for 16 beam tubes; these end plates could therefore be difficult to design and assemble.
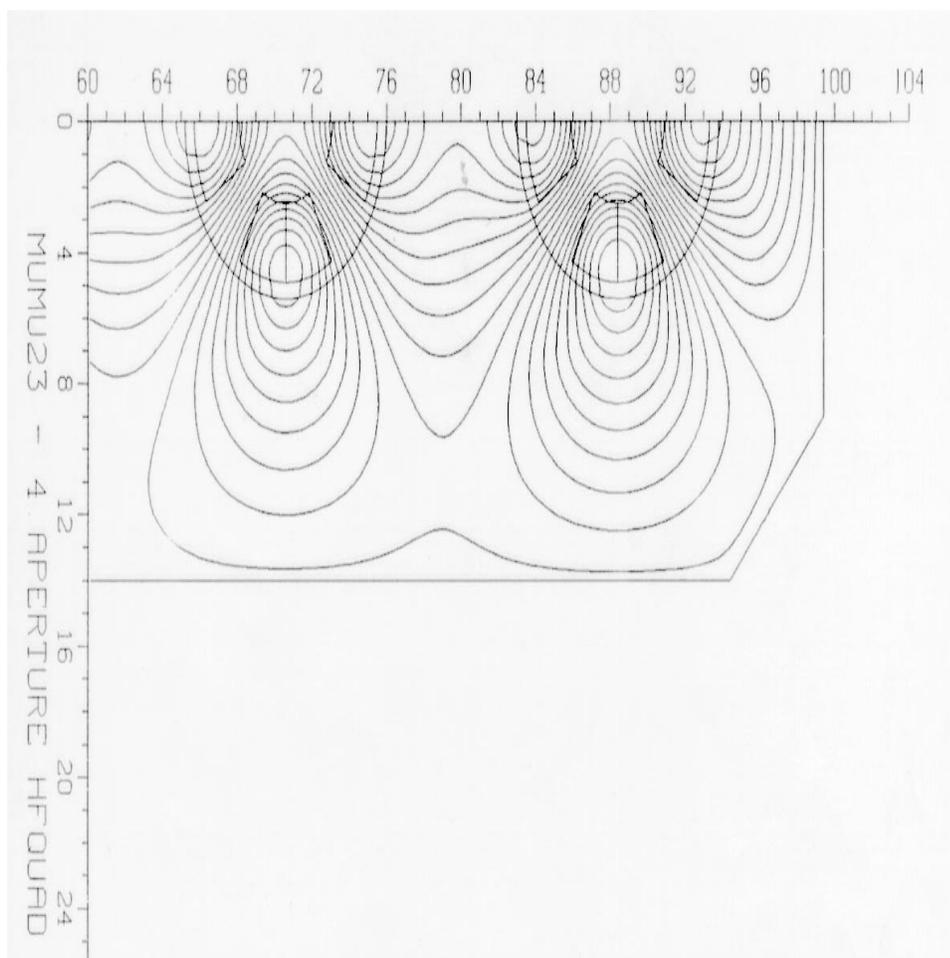
Figure 7.11: Field lines in a quadrant of the highest field dipole and quadrupole stack of the 16 aperture dipole.

Fig.7.11a shows the field lines in the high field dipole stack. A similar stacked-aperture design is possible for the quadrupoles. Fig.7.11b shows the right half of the topmost quad aperture, and half of the next lower aperture, in a 5-aperture quadrupole stack with dimen-

sions matched to the dipole stack. The field lines are those resulting from readily achievable current densities in the 30 current blocks. In the highest gradient aperture, the gradient is $175\,\mathrm{Tm}^{-1}$.

An alternative scenario would be to have a separate pressure vessel for each aperture, i.e., up to 16 separate magnets. This would require more power but have less inter-magnet interference, but could still be economic, if the magnets are modularized for minimal cost. Magnet designs for fewer passes are also possible and should be proportionately easier; in Fig.7.12 we show a cross-section of a 3-magnet stack for a 9-pass arc.[18]
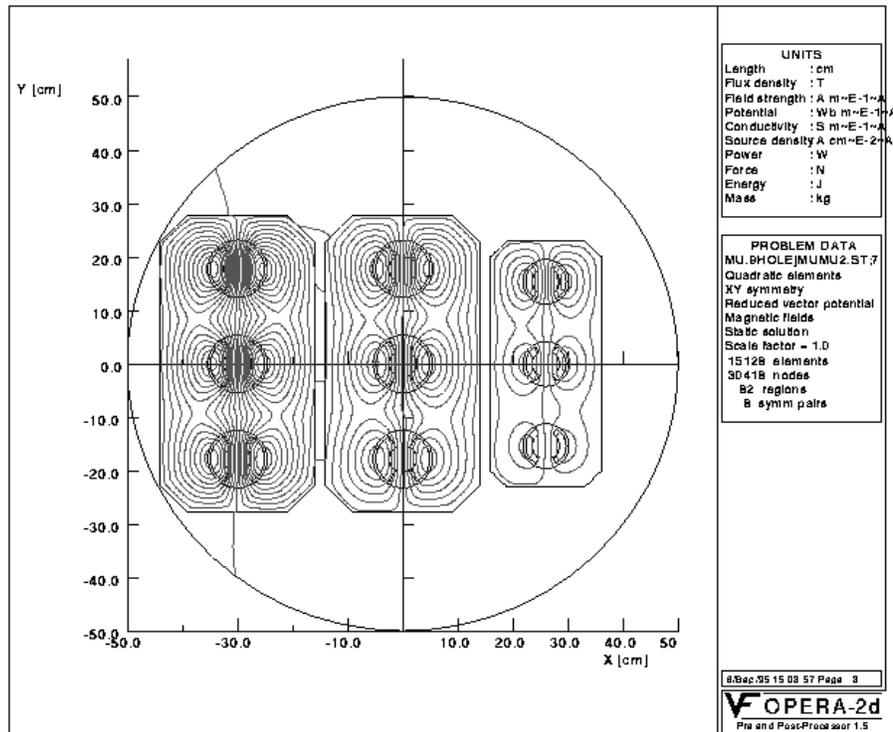
Figure 7.12: A 9 aperture dipole, composed of three stacks of three apertures.

We have used superconducting high-field magnets in this initial design. Other *low-cost* technologies could be used (permanent magnets, super-ferric, etc.), either in combined or separated elements. High field is not required, if the total number of turns remains modest.

Hybrid Magnets

The total length of beam transport, and therefore the cost, could be reduced by cycling the magnetic fields in the return arcs so that the same transport line can be used for multiple

acceleration passes. (In the limit where the same transport line is used for all passes, we obtain the case of a rapid-cycling synchrotron.) However, superconducting magnets cannot cycle at the high rates needed for μ acceleration.

One approach to multipass transport is the use of hybrid magnets, in which rapid-cycling and superconducting high-field magnetic elements are mixed and pulsed so that several passes can go through the same transport.
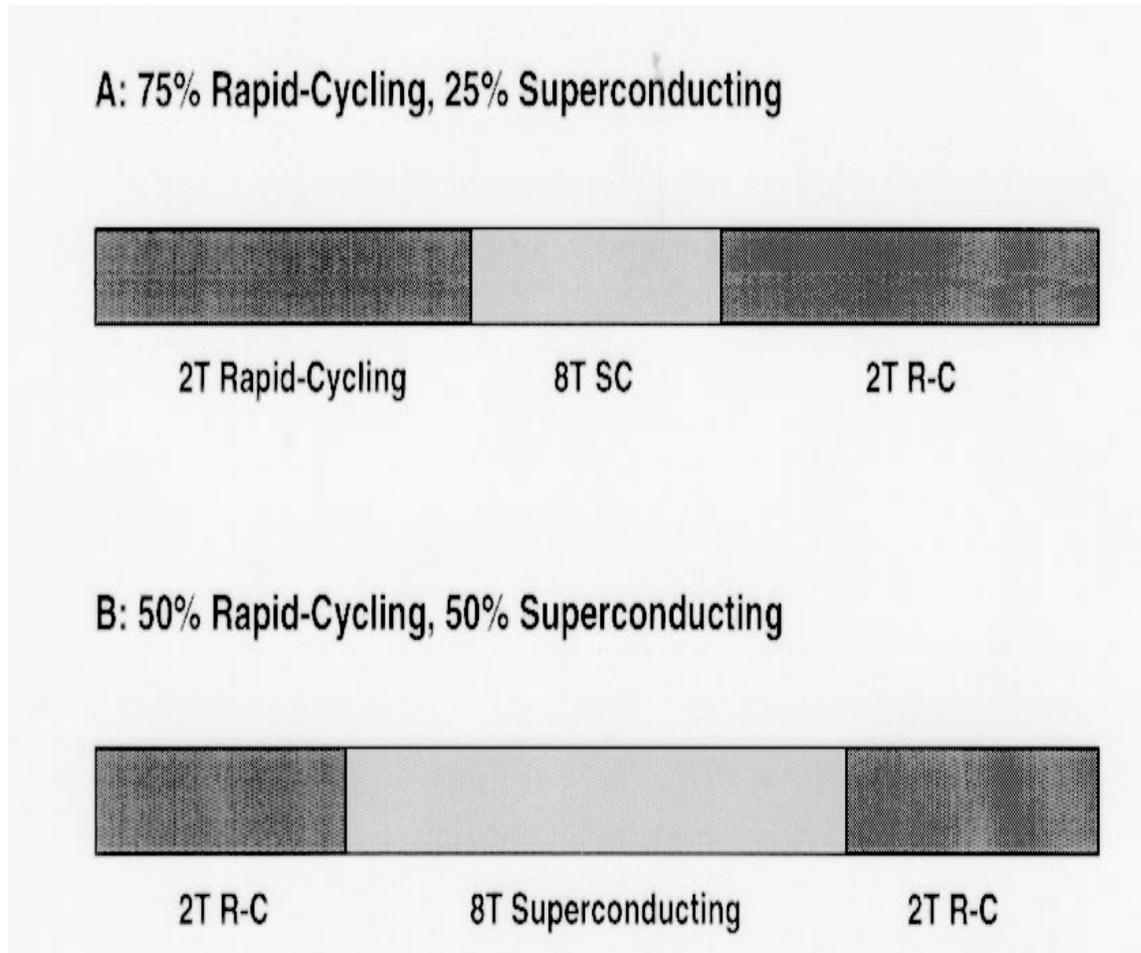

Figure 7.13: Configurations for hybrid rapid-cycling dipoles.

Figure 7.13 shows potential layouts for hybrid magnets, in which high-field magnets are surrounded by rapid-cycling magnets. In this case the rapid-cycling magnets are iron-dominated, and can cycle from $-2T$ to $+2T$, while the superconducting section is fixed at $8T$. Fig.7.13b shows a design with 50% high-field and 50% rapid-cycling, so the mean field can increase from $3.0T$ to $5.0T$, Fig.7.13a shows a design with 25% $8T$ and 75% $12.0T$ rapid-cycling; it would take the mean field from $0.5T$ to $3.5T$. Thus a sequence of two arcs of compound magnets can accommodate acceleration by almost an order of magnitude, which

is what is needed in the accelerators. One can also design compound magnets to obtain 3 or 4 arc versions, with extended capabilities.

A significant problem is the large degree of orbit variation within a magnet unit as the matched beam energy changes, because of the differential bending between the outer cycling magnets and the fixed inner magnets. In the first of the above two cases, we obtain a variation of the central orbit of 5 mm for a 10 m compound magnet with a total bend of 0.0075 radians (2 TeV). In the second case, which has a factor of 5 energy change, the same bend produces an orbit change of 3.3 cm within the cycle. While somewhat extended, these orbit changes are not impossibly large, and magnets can be designed to accommodate them. In the following section these magnet-cycling possibilities are extended to obtain rapid-cycling magnets for rapid-cycling synchrotron scenarios.[20]

7.8   Other Acceleration Scenarios

In this section, we discuss other methods of acceleration than the recirculating linac scenarios and their extensions discussed above. These are all various approaches to obtaining a rapid-cycling synchrotron acceleration. Since all multiturn methods are constrained by the lifetime to $N_{\text{turns}} << 300\,B$, relatively large rf systems are still required. However, major cost savings could be obtained in the elimination of multi-pass transport systems by using transports with changing magnetic fields. Cycling magnetic fields at the rate needed for μ acceleration is a significant challenge and requires untested approaches. However we have identified some possible methods, which we describe below.

7.8.1   Pulsed Dipoles

Magnets that are ramped up quickly in field as the muons gain energy in multi-pass linacs can be used in rapid-cycling acceleration of the beam.[21] A pulsed magnet scheme appears feasible for a 250 GeV machine, but the parameters appear less favorable for a 2 TeV machine. A particular design for a pulsed dipole magnet with parameters chosen to be practical is shown in Figs.7.14 and 7.15, and some parameters are displayed in Tb.7.5. Fig.7.14 shows a quarter of the magnet, in which four turns of multistrand copper formed into a trapezoidal shape are used in each of two required coils. The turns are placed in an approximate $\cos\theta$ current distribution to maximize the field and minimize unwanted harmonics. The iron yoke contributes substantially to the field and provides mechanical support. Cooling requirements are modest and can be satisfied by circulating water in pipes (not shown) passing through the yoke. The magnet shown in Fig.7.14 produces a field of 4 T at a current of 29.5 kA.

Table 7.5: Parameters for pulsed conductor-dominated accelerator and storage ring dipoles

Parameter	unit	Accelerator Dipole	Storage Ring Dipole
Coil inner radius	cm	2	2
Magnet length	m	10	10
Field	T	4	6
Current	kA	29.5	24.9
Stored energy	kJ	160	360
Inductance	mH	0.37	1.2
Coil resistance	mW	19	44
Ramp time, 10% to 90%	μs	360	
Store Time (for 250 GeV)	μs		5000
Power supply voltage	kV	31.2	1.1
Power into magnet 2 Hz	kW	19	452
Power into 250 GeV ring	MW	2.7	39.4

The conductor cross sectional area is $1.275 \, \text{cm}^2$. For a magnet length of 10 m, the inductance is 0.37 mH and the resistance is 19 mW. If 250 GeV corresponds to 90% of full field, a total of 146 such dipoles is required.

Assuming two linacs with a length of 313 m each and an accelerating gradient of 9 MeV/m, and a dipole filling factor of 70% in the arcs, the time required to accelerate the muons from 25 GeV to 250 GeV is $360 \, \mu s$ (40 turns). The power to drive the magnet during this acceleration time can come from the discharge of the stored energy in a capacitor bank. A design with such an LRC power supply, producing the waveform shown in Fig.7.16, has a quarter period of $550 \, \mu s$. Note that the required acceleration is not linear but follows the sinusoidal field increase in the magnets. The voltage required is 31.2 kV and the required storage capacitance is $340 \, \mu F$. Each magnet has its own power supply and it is triggered to discharge in synchronization with the acceleration cycle. After a quarter cycle, the energy is recovered by the power supply in the next quarter cycle, with an efficiency of $\approx 80\%$.

The required voltage (31.2 kV) is uncomfortably high. It can be reduced by connecting some or all of the turns in the magnet in parallel, fed from separate subsections in the power supply. Power supplies with power output similar to that required here operating
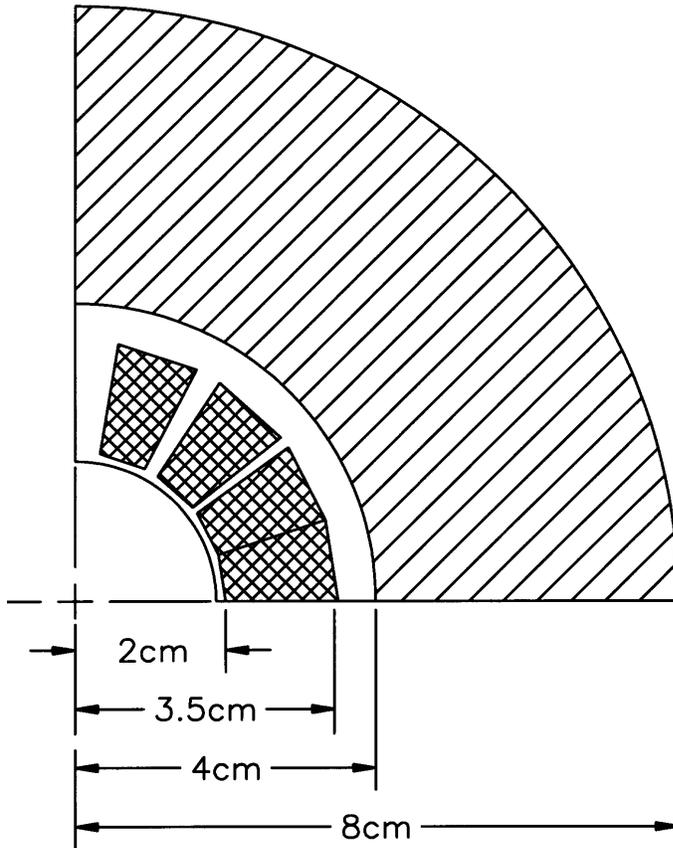
Figure 7.14: Cross sections of pulsed current dipoles for a μ rapid-cycling accelerator dipole (4 T).

at voltages 5 kV are used at accelerators to inject beam or to capture antiprotons in fast kickers.[21] During a half-cycle, the heat deposited in the coils is 9400 J. This gives an estimated temperature rise per cycle in the coils of 0.13 C. At a repetition rate of 2 Hz, the average power dissipated in each magnet due to this resistive heating is 19 kW. For the entire machine (144 dipole magnets), the power dissipated in these magnets at 2 Hz is 2.7 MW. Tb.7.5 includes the parameters for this particular design. The calculations used to obtain these values are approximations and further work will be needed to refine the results.

A similar design approach using pulsed magnets can also be considered for the collider ring. Here, the magnet current need not rise as quickly, but the magnet must have a constant flat-top current for 5 ms for 250 GeV collisions. A possible design is also shown in Fig.7.15. With two layers of turns, a field of 6 T can be achieved. With a dipole filling factor of 0.7, the time for 1000 orbits is 4.2 ms. A current of 24.6 kA and a voltage of 1.1 kV is required
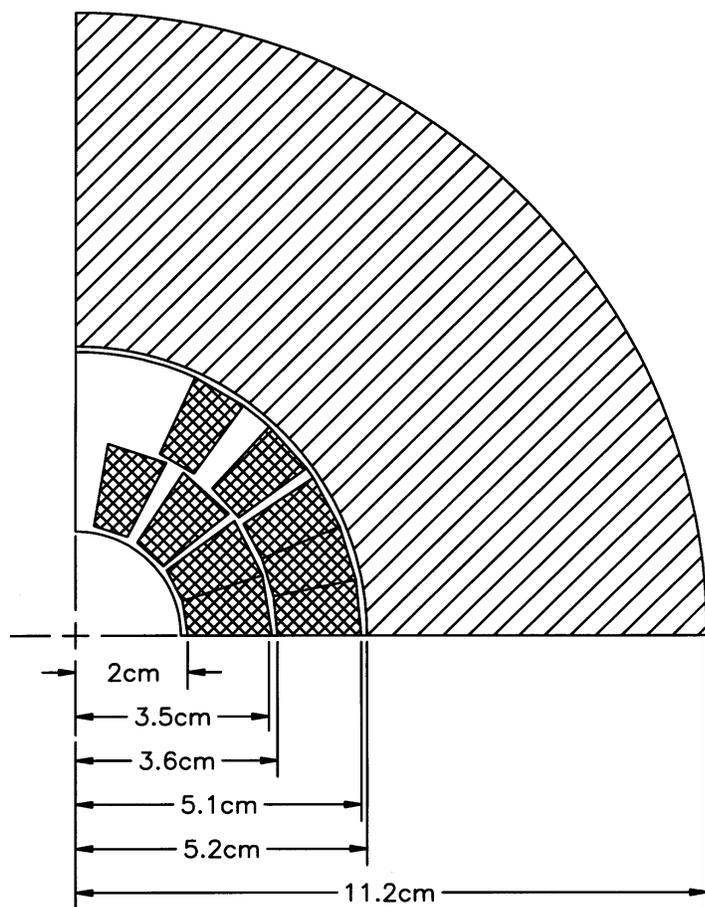
Figure 7.15: Cross sections of pulsed current dipoles for a collider dipole (6 T).

to maintain the current in the magnet. The average power in each magnet at 2 Hz is 452 kW. For the entire ring, with 144 10 m long magnets, the average power at 2 Hz is 39.4 MW. Tb.7.5 includes the parameters of such a design. Note that a pulsed storage ring is not required; the rapid-cycling accelerator could instead fill a fixed-field superconducting ring.

Rapid-cycling dipoles and hybrid rapid-cycling/high-field

Rapid-cycling iron dominated magnets are an established technology but are limited to 60 Hz repetition rates and 2T fields, and both of these parameters are somewhat lower than those desired for μ acceleration. We propose some possible extensions of existing technology to meet this challenge.

An increase in average B-field can be obtained by interlacing fixed-high-field dipoles with ramping magnets, and the range of magnetic field change can be extended by ramping the dipoles fully from -2T to +2T. The ramp rate must also be increased. Scaling from
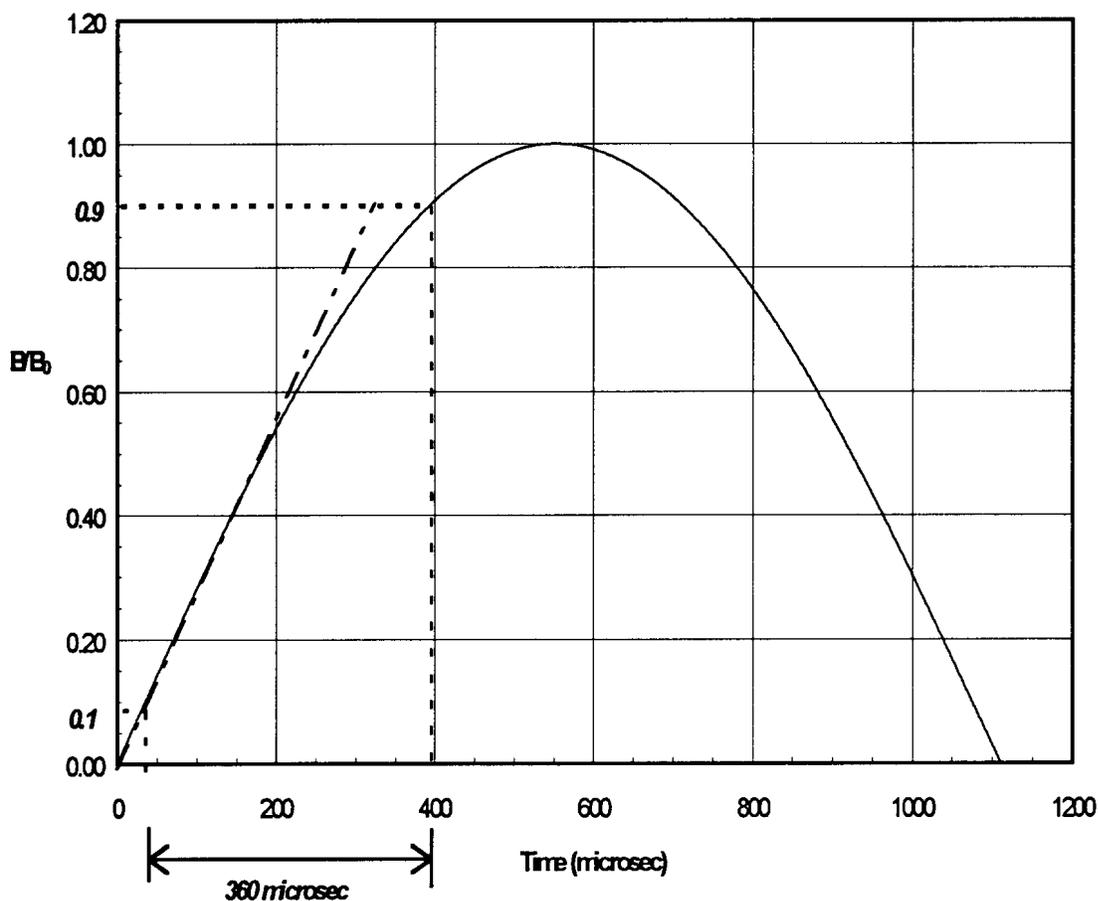
Figure 7.16: Ramp for rapid-cycling pulsed-dipoles for acceleration to 250 GeV.

the KAON booster dipole (50 Hz)[22], design concepts for 250 and 125 Hz μ accelerator dipoles have been developed. In this design concept, the gap within the dipoles is a 8×3 cm rectangle and a high-B ferrite such as supermendur (2%V 49%Fe 49%Co) is used on the pole tips to get the peak field up to $2\,T$. Eddy currents are reduced by the use of 0.1 mm thick laminations (instead of 0.47 mm), and hysteresis losses are reduced by using grain-oriented silicon steel. A 6-turn 4×10 cm Copper conductor (with 0.5 mm square conductor wires) is used, with stainless steel cooling tubes. Power requirements are formidable in these rapid-cycling magnets; a $6\,m$ dipole requires 35/60 kW for 125/250 Hz, respectively.

These rapid-cycling magnets have been combined with $8\,T$ high-field superconducting magnets, in configurations similar to those of Fig.7.13, to form the basis for the rapid-cycling μ accelerator design presented in Tb.7.5, and shown in Fig.7.17. That design consists of two hybrid recirculating linacs, which accelerate the beam from 105 to 730 to 2000 GeV using 250 and 125 Hz dipoles respectively. With an overall dipole occupancy of 70% (split between 2T
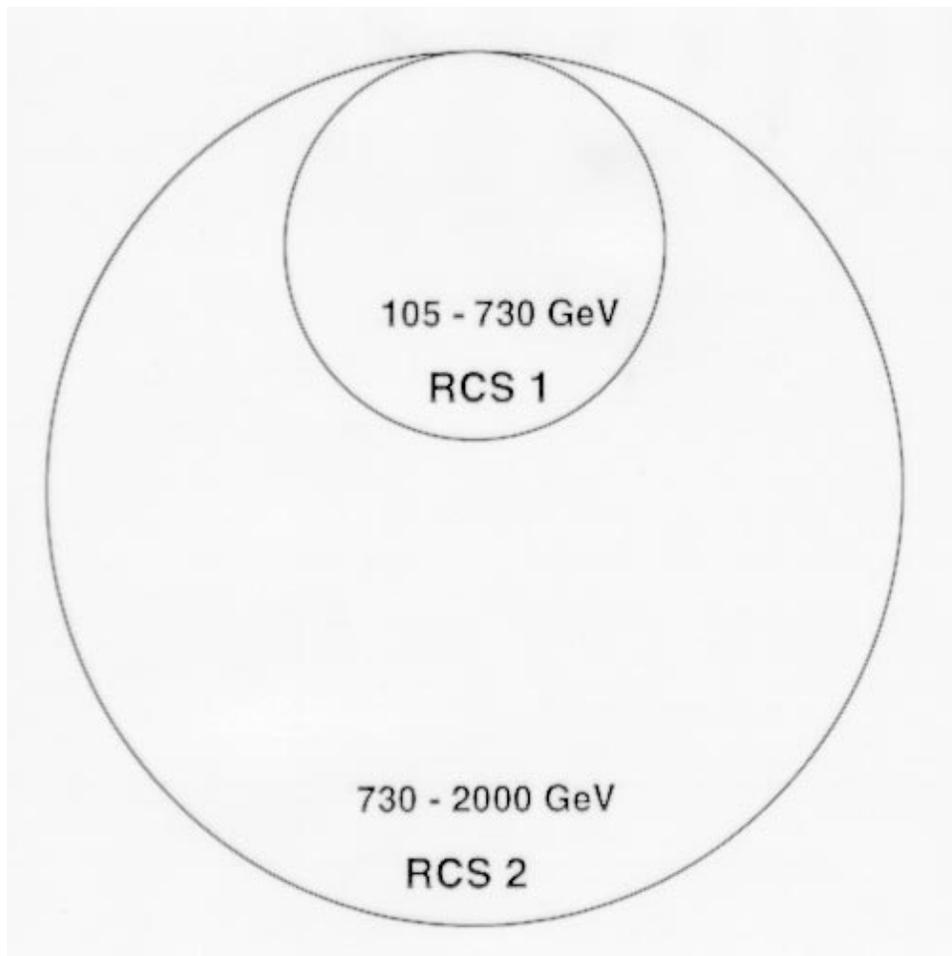
Figure 7.17: Sequence of two rapid-cycling synchrotrons for acceleration from 100 GeV to 2 TeV.

RC and 8T SC units), we obtain 1000 m and 2300 m mean radii for the two rings. (Focusing could be obtained by rapid-cycling (non-hybrid) quadrupoles, which would cycle from low-field to 2T pole-tip fields.) Each accelerator reaches full energy in 100 turns, requiring 6.5 and 15.3 GV rf, respectively. Decay during acceleration is less than 20% per ring. Thus the rf structure requirements are dramatically less than for RLA systems, and only one transport path per ring is required. These advantages are balanced by the very large power requirements of the continuously rapid-cycling magnets (almost 100 MW). This power could be reduced by an order of magnitude, if the power could be gated to pulses matched to the μ collider cycle time (30 Hz), and could be further reduced if the cycle rate was reduced, as was discussed for the pulsed-conductor magnets of the previous section.

Table 7.6: Parameters for a 2 TeV Rapid-Cycling Hybrid Accelerator. The accelerator consists of two rapid-cycling synchrotrons; one takes the beam from 105 to 730 GeV, and a second that takes the beam up to 2 TeV.

Parameter	Symbol	RCS 1	RCS 2
Radius	R	1000	2300 m
Initial Energy	E_i	105	730 GeV
Final Energy	E_f	730	2000 GeV
Ramp frequency	f_F	250	125 Hz
Acceleration orbits	N_t	96	83
rf Voltage	V_{rf}	6.5	15.3 GV
Dipole B field (ave.)	B	$0.5 - 3.5$	$1.5 - 4.1$ T
Dipole composition	(2T RC/8T SC)	75%/25%	65%/35%
RCS Dipole power (cw)	P_{cw}	35 MW	32 MW
RCS Dipole power(30 Hz)	P_{pulsed}	4.5 MW	8 MW
Beam Decay Loss	η_L	26%	14%

7.8.2 Rotating Dipoles/Magnets

The disadvantage of high power rapid-cycling magnets can be reduced, if instead of cycling currents, we rotate the dipoles to obtain a rapid-cycling field. Two adjacent permanent-magnet 2T dipoles counter- rotating at 250 Hz (15,000 rpm) produce a sum field which cycles from -2T to +2 T . Mechanical rotations of this rate, or even faster, are readily obtained using current technology.

The dipoles would be constructed of a radiation-hard material, such as samarium-cobalt, placed in a Halbach *magic-ring* configuration.[23] The interior field is uniform and can exceed the remanent field of the rare earth material: $B = B_r \ln(OD/ID)$, where B_r is the remanent field (1.15 T for samarium cobalt, but 1.3 T for Alnico). 2 T is obtained for Sm_2Co_{17} with outer diameter (OD) of 9 cm and inner diameter (ID) of 1.5 cm. Counter-rotating magic-ring dipoles would have an average field which would cycle between - 2 T and +2 T. These counter-rotating dipoles could be used in place of the rapid-cycling magnets in the rapid-cycling synchrotrons of Tb.7.6, and would greatly reduce power requirements. Substantial problems may exist in this untested configuration. Radiation damage of permanent magnet materials is a concern. The rotating magnets have localized vertical bends in the cycle which

may cause emittance dilution, coupling or even instability. We have not included focusing elements, but counter-rotating permanent magnet quadrupoles could be used. To avoid air friction the magnets will rotate within a vacuum; which would then also be the beam vacuum system. One is concerned whether the rotation might demagnetize the material. Considerable study and tests are needed for this unconventional possibility.

7.9 Comments and Conclusions

We have presented a candidate scenario for a high-energy $\mu^+ - \mu^-$ accelerator. That scenario is based on a multi-stage RLA approach, and it includes a proof-of-principle calculation of the design concept. Much further optimization and design development is needed, and we can identify some of these development goals:

- The bunch-compression and acceleration scenario should be further optimized and simulated.

- Complete lattices are needed, with designs for the transport arcs, including beam separation and recombination.

- An accurate cost algorithm for rf and beam transport components is needed.

- Matching from the output of the μ cooling system to the initial acceleration should be more clearly defined with reoptimization of final cooling and initial acceleration. A consistent injector linac should be specified.

- rf acceleration development is needed, both in the low-frequency rf systems needed in the first stages and in the high- frequency SRF needed in the high-energy accelerators.

- Variations using rapid-cycling should be considered and studied. Prototype rapid-cycling magnet components could be designed and built.

Bibliography

[1] R. Palmer et al.,*Muon Colliders*, Proceedings of the 9th Advanced ICFA Beam Dynamics Workshop, Ed. J. C. Gallardo, AIP Conference Proceedings 372 (1996).

[2] D. Neuffer, *Acceleration to Collisions for the $\mu^+\mu^-$ Collider*, ibid.

[3] D. Neuffer, *Analysis and Simulations of Longitudinal Motion in μ-Recirculating Linacs*, to be published in Nucl. Inst.and Meth. A, 1996.

[4] H. Kirk, presentation to the 9th Advanced ICFA beam Dynamics Workshop 1996, unpublished.

[5] Z. Qian, unpublished (1996).

[6] H. Lengeler, in Proc. 5th General Accelerator Physics Course, S. Turner, ed. CERN 94-01, p. 791 (1994).

[7] G. Cavallari et al., in Proc. 5th Workshop on rf Superconductivity, DESY M92-01, p. 23 (1992).

[8] C. Benvenuti, in Proc. 5th Workshop on rf Superconductivity, DESY M92-01, p. 189 (1992).

[9] G. Spalek and H. A. Thiessen, Proc. 5th Workshop on rf Superconductivity, DESY M92-01, p. 95 (1992).

[10] H. A. Thiessen, private communication (1996).

[11] Q-S Shu for the TESLA collaboration, presented at the CEC/ICMC Conf, Columbus, July 1995.

[12] TESLA-Collaboration - D. Edwards, ed., TESLA Test Facility Linac - Design Report, TESLA 95-01 (1995).

[13] Q.-S. Shu et al., *Experimental Investigation of Quenches in Superfluid He of TESLA 9-Cell Superconducting Cavities*, Proc. 7th RF Superconductivity Workshop, Saclay, France, Oct 16-20, 1995.

[14] A. Mosnier and O. Napoly, Proc. XV Int. Conf. on High Energy Accelerators, J. Rossbach, ed., p. 963 (1992)

[15] Laser Processing Consortium, Free Electron Lasers for Industry Volume 2: UV Demo Conceptual Design, CEBAF, May 1995.

[16] S. Y. Lee, K. Y. Ng, and D. Trbojevic, Phys. Rev. **E 48**, 3040 (1993).

[17] CEBAF Design Report, CEBAF, Newport News VA (1986), unpublished.

[18] S. Kahn, G. Morgan, and E. Willen, *Recirculating arc dipole for the $2 + 2\,\mathrm{TeV}$ $\mu^+\mu^-$ Collider*, Proceedings of the 9th Advanced ICFA Beam Dynamics Workshop, Ed. J. C. Gallardo, AIP Conference Proceedings 372 (1996).

[19] D. Summers, to be published in Proceedings of the Symposium on Physical Potential and Development of Muon-Muon Colliders, San Francisco, CA, Dec. 1995.

[20] E. Willen, *Pulsed dipole Magnets for the Muon Collider*, Magnet Note 555-31, BNL, May 1996.

[21] R. Winje and K. Bourkland, IEEE Trans. Nuc. Sci., NS-22, No.3 (1975), 1242

[22] TRIUMF-KAON FACTORY STUDY Accelerator Design Report, unpublished (1990).

[23] K. Halbach, *Design of Permanent Multipole Magnets with Oriented Rare Earth Cobalt Material*, Nucl. Instr. Meth. 169 (1980) 1.

Contributors

- D. Neuffer, (FermiLab) Editor

- C. Ankenbrandt, (FermiLab)

- A. McInturff, (FermiLab)

- G. Morgan, (BNL)

- Q-S Shu, (CEBAF)

- S. Simrock, (CEBAF)

- D. Summers, (Univ. of Mississippi)

List of Figures

List of Tables